

Cell competition with normal epithelial cells promotes apical extrusion of transformed cells through metabolic changes

Shunsuke Kon^{1*}, Kojiro Ishibashi^{1*}, Hiroto Katoh¹, Sho Kitamoto¹, Takanobu Shirai¹, Shinya Tanaka¹, Mihoko Kajita¹, Susumu Ishikawa¹, Hajime Yamauchi¹, Yuta Yako¹, Tomoko Kamasaki¹, Tomohiro Matsumoto¹, Hirotaka Watanabe¹, Riku Egami¹, Ayana Sasaki¹, Atsuko Nishikawa¹, Ikumi Kameda¹, Takeshi Maruyama¹, Rika Narumi¹, Tomoko Morita¹, Yoshiteru Sasaki², Ryosuke Enoki^{3,4,5}, Sato Honma⁴, Hiromi Imamura⁶, Masanobu Oshima⁷, Tomoyoshi Soga⁸, Jun-ichi Miyazaki⁹, Michael R Duchon¹⁰, Jin-Min Nam¹¹, Yasuhito Onodera¹², Shingo Yoshioka¹³, Junichi Kikuta¹³, Masaru Ishii¹³, Masamichi Imajo¹⁴, Eisuke Nishida¹⁵, Yoichiro Fujioka¹⁶, Yusuke Ohba¹⁶, Toshiro Sato¹⁷ & Yasuyuki Fujita¹

¹Division of Molecular Oncology, Institute for Genetic Medicine, Hokkaido University Graduate School of Chemical Sciences and Engineering, Sapporo 060-0815, Japan.

²Department of Molecular and Cellular Physiology, Graduate School of Medicine, Kyoto University, Kyoto 606-8501, Japan.

³Photonic Bioimaging Section, Research Center for Cooperative projects, Hokkaido University Graduate School of Medicine, Sapporo 060-8638, Japan.

⁴Department of Chronomedicine, Hokkaido University Graduate School of Medicine, Sapporo 060-0810, Japan.

⁵Precursory Research for Embryonic Science and Technology (PRESTO), Japan, Science and Technology Agency (JST), Saitama 332-0012, Japan.

25 ⁶Laboratory of Functional Biology, Graduate School of Biostudies, Kyoto University,
26 Kyoto 606-8501, Japan.

27 ⁷Division of Genetics, Cancer Research Institute, Kanazawa University, Kanazawa
28 920-1192, Japan.

29 ⁸Institute for Advanced Biosciences, Keio University, Tsuruoka 997-0052, Japan.

30 ⁹Department of Nutrition and Physiological Chemistry, Osaka University Medical
31 School, Osaka 565-0871, Japan.

32 ¹⁰Research Department of Cell & Developmental Biology, University College London,
33 London WC1E 6BT, UK.

34 ¹¹Global Station for Quantum Medical Science and Engineering, Global Institution for
35 Collaborative Research and Education (GI-CoRE), Hokkaido University, Sapporo
36 060-8648, Japan.

37 ¹²Department of Molecular Biology, Hokkaido University Graduate School of
38 Medicine, Sapporo 060-8638, Japan.

39 ¹³Department of Immunology and Cell Biology, Graduate School of Medicine and
40 Frontier Biosciences, Osaka University, Osaka 565-0871, Japan.

41 ¹⁴Laboratory of Bioimaging and Cell Signaling, Graduate School of Biostudies, Kyoto
42 University, Kyoto 606-8315, Japan.

43 ¹⁵Department of Cell and Developmental Biology, Graduate School of Biostudies,
44 Kyoto University, Kyoto 606-8502, Japan.

45 ¹⁶Department of Cell Physiology, Hokkaido University Graduate School of Medicine,
46 Sapporo 060-8638, Japan.

47 ¹⁷Department of Gastroenterology, Keio University School of Medicine, Tokyo 160-
48 0016, Japan.

49 *These authors contributed equally to this work.

50

51 **ABSTRACT**

52

53 **Recent studies have revealed that newly emerging transformed cells are often**
54 **apically extruded from epithelial tissues. During this process, normal epithelial**
55 **cells can recognize and actively eliminate transformed cells, a process called**
56 **Epithelial Defence Against Cancer (EDAC). Here, we show that mitochondrial**
57 **membrane potential is diminished in RasV12-transformed cells when they are**
58 **surrounded by normal cells. In addition, glucose-uptake is elevated, leading to**
59 **higher lactate production. The mitochondrial dysfunction is driven by**
60 **upregulation of pyruvate dehydrogenase kinase 4, which positively regulates**
61 **elimination of RasV12-transformed cells. Furthermore, EDAC from the**
62 **surrounding normal cells, involving Filamin, drives the Warburg effect-like**
63 **metabolic alteration. Moreover, using a cell competition mouse model, we**
64 **demonstrate that PDK-mediated metabolic changes promote the elimination of**
65 **RasV12-transformed cells from intestinal epithelia. These data indicate that non-**
66 **cell-autonomous metabolic modulation is a crucial regulator for cell competition,**
67 **shedding light on the unexplored events at the initial stage of carcinogenesis.**

68

69 INTRODUCTION

70

71 It remains enigmatic what happens at the initial stage of carcinogenesis where
 72 oncogenic transformation occurs in a single cell within the epithelium¹⁻³. Recent
 73 studies have demonstrated that newly emerging transformed cells are often eliminated
 74 from epithelial tissues via cell competition against the neighbouring normal epithelial
 75 cells. Cell competition is a process by which two different cell populations, upon
 76 interaction, compete with each other for survival and space; consequently, the loser
 77 cells are eliminated from the tissues, while the winner cells occupy the vacant spaces.
 78 This phenomenon was originally found and has been extensively studied in
 79 *Drosophila*⁴⁻⁹. But, recent studies have revealed that cell competition can also occur in
 80 mammals between normal and various types of transformed epithelial cells. For
 81 example, RasV12-, Src- or erbB2-transformed cells are apically extruded when they
 82 are surrounded by normal epithelial cells¹⁰⁻¹³. In addition, tumour suppressor protein
 83 Scribble- or Mahjong-knockdown cells undergo apoptosis and leave a monolayer of
 84 normal epithelial cells^{7, 14}. Importantly, when transformed cells alone are present,
 85 neither apical extrusion nor apoptosis occurs, indicating that the presence of the
 86 surrounding normal cells profoundly influences the behaviour and fate of transformed
 87 cells.

88 We and other groups have explored the molecular mechanisms of cell competition
 89 between normal and RasV12-transformed epithelial cells and revealed that various
 90 non-cell-autonomous changes occur in both cells at their interface. For instance,
 91 normal epithelial cells accumulate cytoskeletal protein Filamin at the interface with
 92 the adjacent transformed cells, thereby actively eliminating them¹⁵. This implies a
 93 notion that normal epithelial cells have anti-tumour activity that does not involve

94 immune cells: a process termed EDAC (Epithelial Defence Against Cancer)¹⁵. By
95 contrast, in RasV12-transformed cells that are surrounded by normal cells, actin-
96 binding protein Epithelial Protein Lost In Neoplasm (EPLIN) is accumulated¹⁶. The
97 accumulated EPLIN then activates the downstream molecules such as PKA and
98 myosin-II, which positively regulate apical extrusion of RasV12 cells. However, the
99 molecular mechanisms of how EDAC from normal cells affects the neighbouring
100 transformed cells and promotes their elimination are still poorly understood.

101 Cellular metabolism is dynamically modulated and adjusted in accordance with
102 various conditions. For example, at the later stage of cancer development, aerobic
103 glycolysis is enhanced in tumour cells, often accompanied by the downregulation of
104 mitochondrial activity; these metabolic changes are called Warburg effect¹⁷⁻²¹. But, it
105 is not clearly understood whether cellular metabolism is also affected at the initial
106 stage of carcinogenesis. In this study, we have examined whether and how the
107 metabolic status is regulated at the interface between normal and newly emerging
108 transformed epithelial cells.

109

110 RESULTS

111 Warburg effect-like metabolic changes occur in RasV12-transformed cells that 112 are surrounded by normal cells

113 To examine the involvement of metabolic regulation in cell competition, we first
114 examined mitochondrial energy metabolism at the interface between normal and
115 RasV12-transformed epithelial cells. TMRM (tetramethylrhodamine methyl ester) is a
116 positively charged red fluorescent dye that accumulates in active mitochondria
117 according to the negative membrane potential gradient across their inner membranes.
118 We found that the TMRM fluorescence, but not the fluorescence of a control dye
119 CMTPX, was strongly reduced in RasV12-transformed epithelial cells surrounded by
120 normal epithelial cells compared to that in RasV12-transformed cells cultured alone
121 or in GFP-expressing cells surrounded by normal cells (Fig. 1a-c, g). The comparable
122 phenomenon was also observed in Src-transformed cells, but not in Scribble-
123 knockdown cells (Supplementary Fig. 1a, b). The decreased incorporation of TMRM
124 was observed in both apically extruding and extruded RasV12 cells (Fig. 1d). The mix
125 ratio of normal and RasV12 cells affected the TMRM incorporation in RasV12 cells;
126 the decreased TMRM incorporation was clearly observed at 50:1 or 10:1, but less
127 frequently occurred at 4:1 or 1:1. This is compatible with the previous report
128 demonstrating that the proportion of winner-loser cells profoundly influences the
129 occurrence of cell competition²². The non-cell-autonomous downregulation of
130 mitochondrial membrane potential was also confirmed by using mitoSOX, an
131 indicator for mitochondrial superoxide production that reflects mitochondrial ATP
132 production (Fig. 1e-g). Immunofluorescence of the mitochondrial resident protein
133 Tom20 or MitoTracker Green fluorescence which is incorporated into mitochondria in
134 a membrane potential-independent manner showed that the number of mitochondria

was not altered in RasV12 cells surrounded by normal cells (Fig. 1h and Supplementary Fig. 1c-h). In addition, by electron microscopic analyses, mitophagosome-like structures were frequently observed in RasV12 cells that were surrounded by normal epithelial cells (Supplementary Fig. 2). Collectively, these data imply that the decreased TMRM incorporation does not result from a change in mitochondrial mass, but from a change in mitochondrial function. Furthermore, we found that incorporation of glucose analogue 2-NBDG was enhanced in RasV12 cells surrounded by normal cells (Fig. 2a, b), suggesting that uptake of glucose is enhanced in a non-cell-autonomous fashion. Moreover, expression of LDHA, which converts pyruvate to lactate, was significantly increased in RasV12-transformed cells that were surrounded by normal cells (Fig. 2c-e and Supplementary Fig. 3a). Accordingly, lactate secretion was higher in RasV12 cells than normal cells, and was further enhanced when RasV12 cells were surrounded by normal cells (Fig. 2f). This non-cell-autonomous increase in lactate secretion was abolished when LDHA was knocked down in RasV12 cells (Fig. 2f and Supplementary Fig. 4e). These data indicate that the interaction with the neighbouring normal epithelial cells potentiates the Warburg effect-like metabolic changes in transformed cells: downregulation of mitochondrial function and enhanced aerobic glycolysis.

PDK4 plays a crucial role in the decreased mitochondrial membrane potential and apical extrusion of RasV12-transformed cells surrounded by normal cells

To reveal the molecular mechanism that causes the Warburg effect-like phenomenon, we examined expression of various metabolic enzymes by quantitative real-time PCR and found that expression of pyruvate dehydrogenase kinase 4 (PDK4) was significantly elevated in RasV12-transformed cells when they were co-cultured with

normal cells (Fig. 3a). PDK4 phosphorylates and thus inactivates pyruvate dehydrogenase (PDH) that catalyses conversion of pyruvate to acetyl-CoA, thereby blocking the entry into the TCA cycle (Supplementary Fig. 3a). Indeed, phosphorylation of PDH was also enhanced in RasV12 cells when they were surrounded by normal cells (Fig. 3b-d). To examine the functional involvement of PDK4, we established RasV12-transformed cells stably expressing PDK4-shRNA (Fig. 3e) and CRISPR-edited PDK4-knockout RasV12-transformed cells (Supplementary Fig. 3b). PDK4-knockdown or PDK4-knockout suppressed PDH phosphorylation and significantly restored TMRM incorporation in RasV12 cells surrounded by normal cells (Fig. 3f, g and Supplementary Fig. 3c-g), suggesting that upregulation of PDK4 is, at least partly, responsible for the decreased mitochondrial membrane potential. PDK4-knockdown or -knockout also suppressed LDHA accumulation (Supplementary Fig. 3h-j). Interestingly, PDK4-knockdown or -knockout drastically suppressed apical extrusion of RasV12 cells, while promoting formation of basal protrusions that extended beneath the neighbouring normal cells (Fig. 3h, i and Supplementary Fig. 3k-n). DCA is a specific inhibitor of the PDK family^{23, 24} of which upregulation is often observed in the later stage of cancer²⁵⁻²⁸. Therefore, DCA has been intensively tested in clinical trials for treatment of malignant cancer including glioblastoma and various solid tumours²⁹⁻³². We found that treatment of DCA caused the comparable effect to that induced by PDK4 knockdown/knockout: suppression of PDH phosphorylation (Fig. 4a), restoration of TMRM incorporation (Fig. 4b, c) and suppression of apical extrusion and promotion of basal protrusions (Fig. 4d, e). We also demonstrated that another PDK inhibitor Radicicol phenocopied the effect of DCA (Supplementary Fig. 4a-d). DCA treatment also suppressed elevated LDHA expression in RasV12 cells surrounded by normal

185 cells (Fig. 4a). In contrast, knockdown of LDHA in RasV12 cells did not affect
 186 TMRM incorporation (Supplementary Fig. 4e, f), suggesting that decreased
 187 mitochondrial membrane potential causes LDHA upregulation. Moreover,
 188 knockdown of LDHA moderately suppressed apical extrusion (Supplementary Fig.
 189 4g). These results imply that the PDK4-mediated Warburg effect-like metabolic
 190 alteration influences the behaviour of transformed cells and promotes their
 191 elimination from epithelia. When PDH-knockdown cells were surrounded by normal
 192 cells, apical extrusion did not occur (Supplementary Fig. 4h-j), indicating that
 193 downregulation of mitochondrial membrane potential alone is not sufficient to cause
 194 apical extrusion. Thus, while the non-cell-autonomously induced metabolic changes
 195 play an indispensable role in the elimination of transformed cells, additional,
 196 unidentified molecular mechanisms are also involved in this process, which need to
 197 be explored in future studies.

198

199 **EDAC and EPLIN act upstream of the Warburg effect-like metabolic changes in** 200 **RasV12 cells surrounded by normal cells**

201 We further examined the molecular mechanism underlying the Warburg effect-like
 202 phenomenon. In a previous study, we demonstrated that EPLIN accumulates in
 203 RasV12-transformed cells surrounded by normal cells and plays a positive role in the
 204 apical extrusion via activation of the downstream molecules, protein kinase A (PKA)
 205 and myosin-II¹⁶. We found that knockdown of EPLIN in RasV12 cells significantly
 206 restored mitochondrial membrane potential (Fig. 5a, b and Supplementary Fig. 5a). In
 207 addition, EPLIN-knockdown suppressed PDK4 upregulation, phosphorylation of
 208 PDH and LDHA accumulation (Fig. 5c, d and Supplementary Fig. 5b). These data
 209 indicate that EPLIN is a crucial upstream regulator of the Warburg effect-like

210 metabolic changes. Furthermore, we examined the effect of various inhibitors on
211 TMRM incorporation and apical extrusion. Concerning downstream molecules of
212 EPLIN, PKA inhibitor KT5720 reverted TMRM incorporation, whereas myosin-II
213 inhibitor Blebbistatin did not (Supplementary Fig. 5c and Supplementary Fig. 8a).
214 The other tested inhibitors (Cytochalasin D, NAC, 3-MA, Y27632, L-NAME) did not
215 affect TMRM incorporation (Supplementary Fig. 5c and Supplementary Fig. 8a),
216 indicating the specific effect of KT5720 on TMRM incorporation. Furthermore,
217 KT5720 did not significantly affect expression of PDK4. These data suggest that
218 EPLIN regulates those metabolic changes via PDK4- and PKA-dependent pathways
219 (Supplementary Fig. 8c).

220 It was previously reported that normal epithelial cells can recognize and actively
221 eliminate the neighbouring transformed cells, in which Filamin in the normal cells
222 plays an important role, at least partly, by inducing the accumulation of EPLIN in
223 transformed cells^{15, 16}; this tumour-suppressing process is called EDAC¹⁵. When
224 RasV12 cells were surrounded by EDAC-deficient Filamin-knockdown cells, TMRM
225 incorporation in RasV12 cells was restored, instead rather promoted in comparison to
226 that in the surrounding knockdown cells (Fig. 5e, f and Supplementary Fig. 3f and
227 5a). In addition, knockdown of Filamin in the surrounding normal cells substantially
228 suppressed phosphorylation of PDH and accumulation of LDHA (Fig. 5g and
229 Supplementary Fig. 3d, i and 5b). Collectively, these data demonstrate that EDAC
230 from normal cells induces the metabolic alterations of the neighbouring transformed
231 cells via EPLIN, thereby promoting elimination of the transformed cells from
232 epithelia (Supplementary Fig. 8c).

233

234 **Upregulation of the glycolytic pathway plays a positive role in the elimination of**
235 **RasV12-transformed cells**

236 What is the functional significance of EDAC-induced Warburg effect-like metabolic
237 changes in the apical elimination of transformed cells? The metabolic shift from
238 mitochondrial oxidative phosphorylation to glycolysis can affect various cellular
239 processes such as glucose metabolism, ATP production and resistance to ROS-
240 mediated oxidative stress. Using a glucose-FRET probe, we found that intracellular
241 glucose concentration was substantially diminished in RasV12 cells surrounded by
242 normal cells (Fig. 6a-c), indicating that intracellular glucose is exhausted via
243 massively elevated glycolysis despite of the increased glucose uptake (Fig. 2a, b). The
244 comparable glucose metabolic condition is also reported in conventional Warburg
245 effect³³⁻³⁵. In addition, the result with the FRET-based ATP sensor (ATeam) showed
246 that the ATP level was moderately increased in RasV12-transformed cells that were
247 surrounded by normal cells (Supplementary Fig. 5d-f), suggesting that the ATP
248 production is fully compensated and even promoted by the enhanced glycolytic
249 pathway. To further understand the functional significance of this process, we
250 examined the effect of a hexokinase inhibitor 2-deoxy-D-glucose (2-DG). Addition of
251 2-DG diminished the non-cell-autonomously upregulated ATP level (Supplementary
252 Fig. 5e-g) and significantly suppressed apical extrusion of RasV12 cells surrounded
253 by normal cells (Supplementary Fig. 5h, i), indicating that the upregulation of the
254 glycolytic pathway plays a positive role in the elimination of transformed cells. The
255 ATP production speed via glycolysis is far greater than that via mitochondria³⁶, hence
256 the metabolic shift to glycolysis may be of benefit to transformed cells by supporting
257 prompt energy supply required for the dynamic process of apical extrusion. Note that
258 2-DG could inhibit both oxidative and fermentative glucose metabolism. To further

clarify the metabolic alterations during apical extrusion, additional experiments are required in future studies.

PDK-mediated mitochondrial dysfunction induces apical elimination of RasV12-transformed cells *ex vivo* and *in vivo*

To understand the generality and functional significance of these findings, we established an LSL-RasV12-IRES-eGFP mouse whereby RasV12 expression is induced in a Cre-dependent fashion and traced by simultaneous expression of eGFP (Supplementary Fig. 6a, b). By crossing a Villin-Cre-ERT2 mouse with an LSL-RasV12-IRES-eGFP mouse, we obtained a cell competition mouse model (Fig. 7a). Administration of a low dose of tamoxifen induces recombination events less frequently, resulting in expression of RasV12 in a mosaic manner within intestinal epithelia (Supplementary Fig. 6c). Using this system, we examined the fate of newly emerging RasV12-transformed cells that are surrounded by normal epithelial cells *ex vivo* and *in vivo*. First, intestinal epithelial cells were collected from these mice and were subjected to crypt organoid culture in the matrigel, followed by tamoxifen treatment³⁷. At 12-24 h after treatment with a low dose of tamoxifen, RasV12-expressing cells were apically shifted with wedge-like morphology; at 36-48 h, RasV12 cells were detached from the basement membrane and eventually extruded into the apical lumen (Fig. 7b, top). In contrast, cells expressing only GFP remained within the epithelium, and apical extrusion did not frequently occur (Fig. 7b, bottom). When RasV12 were predominantly expressed in the whole epithelium by a high dose of tamoxifen, the frequency of apical extrusion was strongly suppressed (Fig. 7c), indicating that the presence of the surrounding normal cells induced the elimination of transformed cells in the *ex vivo* system as well. We also found that EPLIN was

284 accumulated in RasV12 cells surrounded by normal cells in a non-cell-autonomous
285 fashion (Supplementary Fig. 7a). Time-lapse analyses of the crypt organoid culture
286 revealed that the event of apical extrusion took rather variable times between 2-20 h
287 and that the extruded transformed cells disappeared into the apical lumen
288 (Supplementary Fig. 7b and Supplementary Videos 1-3). Thus, we have successfully
289 established a mouse model system, in which apical elimination of RasV12-
290 transformed cells can be captured three-dimensionally. Using this experimental
291 system, we found that TMRM incorporation was diminished in both extruding and
292 extruded RasV12-expressing cells that were surrounded by normal cells (Fig. 7d, first
293 and second upper panels, e), but not in RasV12-expressing cells surrounded by
294 themselves or in GFP-expressing cells (Fig. 7d, third and fourth panels, e). In
295 addition, phosphorylation of PDH was elevated in RasV12 cells surrounded by
296 normal cells (Fig. 7f). Furthermore, DCA treatment restored the TMRM incorporation
297 and suppressed the apical extrusion of RasV12 cells (Fig. 7g, h and Supplementary
298 Fig. 7c, d). Finally, we examined the fate of RasV12-transformed cells *in vivo*.
299 Intraperitoneal injection of a low dose of tamoxifen induced RasV12 expression in a
300 mosaic manner within the intestinal epithelium, and most of RasV12-expressing cells
301 were apically eliminated after three days of tamoxifen treatment, whereas GFP-
302 expressing cells remained in the epithelial layer (Fig. 8a-c). Using two-photon
303 microscopic *in vivo* time-lapse imaging, the dynamic mode of apical extrusion of
304 RasV12-expressing cells was captured (Fig. 8d and Supplementary Video 4). Finally,
305 we examined the functional role of PDK in the elimination of RasV12 cells from
306 epithelia *in vivo*. When DCA was administered, apical extrusion of RasV12 cells was
307 significantly suppressed (Fig. 8e, f). Furthermore, we used the recently established
308 iGT (intestine-specific gene transfer) system where mouse intestinal epithelia can be

309 transfected with siRNA using HVJ-E (haemagglutinating virus of Japan envelope)
310 (Fig. 8g, h)³⁸. We then demonstrated that knockdown of PDK4 significantly
311 suppressed apical extrusion (Fig. 8i-k). Collectively, these data suggest that apical
312 elimination of RasV12-transformed cells occurs *ex vivo* and *in vivo*, which is
313 promoted by the PDK4-mediated mitochondrial downregulation.
314

315 Discussion

316 The glycolytic pathway and mitochondrial function are frequently de-regulated in
317 neoplastic cells in various ways. These metabolic alterations are generally thought to
318 promote cancer progression, though its biological and pathological significance still
319 remains elusive¹⁷⁻²⁰. Indeed, clinical trials targeting derailed mitochondrial
320 metabolism, such as with DCA, are currently undergoing²⁹⁻³². By contrast, our study
321 suggests that the Warburg effect-like metabolic changes can occur at the early stage
322 of carcinogenesis in a non-cell-autonomous fashion and that DCA treatment could
323 potentially suppress eradication of newly emerging transformed cells. Thus, the
324 adverse effect of DCA may need to be carefully re-examined for the longer time
325 periods.

326 The EDAC-mediated Warburg effect-like metabolic shift does not accommodate
327 several features of the prevailing Warburg effect (Supplementary Fig. 8b).
328 Conventional Warburg effect, which is often observed at the relatively late phase of
329 cancer progression, is caused by various genetic and epigenetic insults and adaptation
330 to harsh tumour microenvironments. In contrast, EDAC-induced Warburg effect-like
331 metabolic changes are triggered by the inputs from neighbouring normal cells at the
332 initial stage of carcinogenesis. The conventional Warburg effect is generally
333 associated with upregulation of HIF1, PDK1/3 and PKM2³⁹⁻⁴⁶, whereas in EDAC-
334 induced Warburg effect-like metabolic changes the expression of these enzymes is not
335 elevated, instead EPLIN and PDK4 act as key upstream regulators. Moreover, the
336 most crucial difference between conventional Warburg effect and EDAC-induced
337 metabolic changes is their roles in tumourigenesis; the former generally plays a
338 tumour-promoting role, whereas the latter potentially plays a tumour-suppressive role
339 by actively eliminating transformed cells. Thus, though these two processes share

340 similar metabolic alterations (mitochondrial downregulation and increased aerobic
341 glycolysis), they are governed by distinct upstream and downstream mediators.

342 HIF1 is a crucial regulator for Warburg effect by modulating multiple metabolic
343 pathways including the TCA cycle and glycolytic pathway⁴⁷. Therefore, we explored
344 the involvement of HIF1 in EDAC-induced Warburg effect-like metabolic changes.
345 By using the 5xHRE (HIF1 responsive element) reporter assay, we found that HIF1
346 activity was not enhanced in RasV12 cells surrounded by normal cells, compared with
347 that in RasV12 cells cultured alone (Supplementary Fig. 7e). It has been reported that
348 HIF1 enhances transcription of PDK1/3 and LDHA, thereby inducing Warburg
349 effect⁴⁷. But, qRT-PCR analysis demonstrated that the mRNA level of PDK1/3 or
350 LDHA was not increased in RasV12 cells surrounded by normal cells (Fig. 3a). Thus,
351 we could not obtain evidence showing the involvement of HIF1 in EDAC-induced
352 metabolic changes, and our data suggest that LDHA is post-transcriptionally
353 upregulated by a HIF1-independent, unknown mechanism.

354 In this study, we have mainly used fluorescence imaging to demonstrate the non-
355 cell-autonomous changes between normal and transformed epithelial cells. In the
356 research field of cell competition, the researchers have struggled with the technical
357 problem: biochemical analyses of each cell population in co-cultures. The non-cell-
358 autonomous changes induced by the neighbouring normal cells are regulated
359 temporally and dynamically, thus once the interaction with normal cells is disrupted,
360 the non-cell-autonomous biochemical changes (not the mRNA level) will instantly
361 vanish. To perform biochemical analyses for each cell population, the co-cultured
362 epithelial cells should be first treated with trypsin to disrupt cell-cell adhesions and
363 dissociate cells from each other, which will be then FACS sorted for a few hours.
364 Despite of the substantial number of trials, we have found just minor remaining non-

365 cell-autonomous traces after those procedures. To further intensify the findings in this
366 study, we need to exploit new methods such as FRET probes for metabolites in future
367 studies.

368 A previous study in *Drosophila* has shown that mitochondrial metabolism can be
369 regulated during cell competition⁴⁸. Our data in this study demonstrate that metabolic
370 modulation is a crucial regulator for cell competition between normal and transformed
371 epithelial cells in mammals as well. Further elucidation of the molecular mechanisms
372 that drive the EDAC-induced metabolic changes will lead to novel approaches for
373 cancer prevention.

374

375

376 **References**

- 377 1. Hanahan, D. & Weinberg, R.A. Hallmarks of cancer: the next generation. *Cell*
378 **144**, 646-674 (2011).
- 379 2. Fialkow, P.J. Clonal origin of human tumors. *Biochimica et biophysica acta*
380 **458**, 283-321 (1976).
- 381 3. Nowell, P.C. The clonal evolution of tumor cell populations. *Science* **194**, 23-
382 28 (1976).
- 383 4. Morata, G. & Ripoll, P. Minutes: mutants of drosophila autonomously
384 affecting cell division rate. *Dev Biol* **42**, 211-221 (1975).
- 385 5. de la Cova, C., Abril, M., Bellosta, P., Gallant, P. & Johnston, L.A.
386 Drosophila myc regulates organ size by inducing cell competition. *Cell* **117**,
387 107-116 (2004).
- 388 6. Moreno, E. & Basler, K. dMyc transforms cells into super-competitors. *Cell*
389 **117**, 117-129 (2004).
- 390 7. Tamori, Y. *et al.* Involvement of Lgl and Mahjong/VprBP in cell competition.
391 *PLoS Biol* **8**, e1000422 (2010).
- 392 8. Karim, F.D. & Rubin, G.M. Ectopic expression of activated Ras1 induces
393 hyperplastic growth and increased cell death in Drosophila imaginal tissues.
394 *Development* **125**, 1-9 (1998).
- 395 9. Brumby, A.M. & Richardson, H.E. scribble mutants cooperate with oncogenic
396 Ras or Notch to cause neoplastic overgrowth in Drosophila. *The EMBO*
397 *journal* **22**, 5769-5779 (2003).
- 398 10. Hogan, C. *et al.* Characterization of the interface between normal and
399 transformed epithelial cells. *Nat Cell Biol* **11**, 460-467 (2009).
- 400 11. Kajita, M. *et al.* Interaction with surrounding normal epithelial cells influences
401 signalling pathways and behaviour of Src-transformed cells. *J Cell Sci* **123**,
402 171-180 (2010).
- 403 12. Wu, S.K. *et al.* Cortical F-actin stabilization generates apical-lateral patterns
404 of junctional contractility that integrate cells into epithelia. *Nat Cell Biol* **16**,
405 167-178 (2014).
- 406 13. Leung, C.T. & Brugge, J.S. Outgrowth of single oncogene-expressing cells
407 from suppressive epithelial environments. *Nature* **482**, 410-413 (2012).
- 408 14. Norman, M. *et al.* Loss of Scribble causes cell competition in mammalian
409 cells. *J Cell Sci* **125**, 59-66 (2012).
- 410 15. Kajita, M. *et al.* Filamin acts as a key regulator in epithelial defence against
411 transformed cells. *Nature communications* **5**, 4428 (2014).
- 412 16. Ohoka, A. *et al.* EPLIN is a crucial regulator for extrusion of RasV12-
413 transformed cells. *J Cell Sci* **128**, 781-789 (2015).
- 414 17. Vander Heiden, M.G., Cantley, L.C. & Thompson, C.B. Understanding the
415 Warburg effect: the metabolic requirements of cell proliferation. *Science* **324**,
416 1029-1033 (2009).
- 417 18. Sciacovelli, M., Gaude, E., Hilvo, M. & Frezza, C. The metabolic alterations
418 of cancer cells. *Methods in enzymology* **542**, 1-23 (2014).
- 419 19. Koppenol, W.H., Bounds, P.L. & Dang, C.V. Otto Warburg's contributions to
420 current concepts of cancer metabolism. *Nat Rev Cancer* **11**, 325-337 (2011).
- 421 20. Cairns, R.A., Harris, I.S. & Mak, T.W. Regulation of cancer cell metabolism.
422 *Nat Rev Cancer* **11**, 85-95 (2011).
- 423 21. Warburg, O. On the origin of cancer cells. *Science* **123**, 309-314 (1956).

- 424 22. Levayer, R., Hauert, B. & Moreno, E. Cell mixing induced by myc is required
425 for competitive tissue invasion and destruction. *Nature* **524**, 476-480 (2015).
- 426 23. Kato, M., Li, J., Chuang, J.L. & Chuang, D.T. Distinct structural mechanisms
427 for inhibition of pyruvate dehydrogenase kinase isoforms by AZD7545,
428 dichloroacetate, and radicicol. *Structure* **15**, 992-1004 (2007).
- 429 24. Wynn, R.M. *et al.* Pyruvate dehydrogenase kinase-4 structures reveal a
430 metastable open conformation fostering robust core-free basal activity. *The*
431 *Journal of biological chemistry* **283**, 25305-25315 (2008).
- 432 25. Sutendra, G. *et al.* Mitochondrial activation by inhibition of PDKII suppresses
433 HIF1a signaling and angiogenesis in cancer. *Oncogene* **32**, 1638-1650 (2013).
- 434 26. Koukourakis, M.I. *et al.* Pyruvate dehydrogenase and pyruvate dehydrogenase
435 kinase expression in non small cell lung cancer and tumor-associated stroma.
436 *Neoplasia* **7**, 1-6 (2005).
- 437 27. Hur, H. *et al.* Expression of pyruvate dehydrogenase kinase-1 in gastric cancer
438 as a potential therapeutic target. *International journal of oncology* **42**, 44-54
439 (2013).
- 440 28. Lu, C.W. *et al.* Overexpression of pyruvate dehydrogenase kinase 3 increases
441 drug resistance and early recurrence in colon cancer. *The American journal of*
442 *pathology* **179**, 1405-1414 (2011).
- 443 29. Chu, Q.S. *et al.* A phase I open-labeled, single-arm, dose-escalation, study of
444 dichloroacetate (DCA) in patients with advanced solid tumors. *Investigational*
445 *new drugs* **33**, 603-610 (2015).
- 446 30. Dunbar, E.M. *et al.* Phase 1 trial of dichloroacetate (DCA) in adults with
447 recurrent malignant brain tumors. *Investigational new drugs* **32**, 452-464
448 (2014).
- 449 31. Strum, S.B. *et al.* Case report: Sodium dichloroacetate (DCA) inhibition of the
450 "Warburg Effect" in a human cancer patient: complete response in non-
451 Hodgkin's lymphoma after disease progression with rituximab-CHOP. *Journal*
452 *of bioenergetics and biomembranes* **45**, 307-315 (2013).
- 453 32. Garon, E.B. *et al.* Dichloroacetate should be considered with platinum-based
454 chemotherapy in hypoxic tumors rather than as a single agent in advanced
455 non-small cell lung cancer. *Journal of cancer research and clinical oncology*
456 **140**, 443-452 (2014).
- 457 33. Kami, K. *et al.* Metabolomic profiling of lung and prostate tumor tissues by
458 capillary electrophoresis time-of-flight mass spectrometry. *Metabolomics :*
459 *Official journal of the Metabolomic Society* **9**, 444-453 (2013).
- 460 34. Shestov, A.A. *et al.* Quantitative determinants of aerobic glycolysis identify
461 flux through the enzyme GAPDH as a limiting step. *eLife* **3** (2014).
- 462 35. Tang, X. *et al.* A joint analysis of metabolomics and genetics of breast cancer.
463 *Breast cancer research : BCR* **16**, 415 (2014).
- 464 36. Pfeiffer, T., Schuster, S. & Bonhoeffer, S. Cooperation and competition in the
465 evolution of ATP-producing pathways. *Science* **292**, 504-507 (2001).
- 466 37. Sato, T. *et al.* Single Lgr5 stem cells build crypt-villus structures in vitro
467 without a mesenchymal niche. *Nature* **459**, 262-265 (2009).
- 468 38. Imajo, M., Ebisuya, M. & Nishida, E. Dual role of YAP and TAZ in renewal
469 of the intestinal epithelium. *Nat Cell Biol* **17**, 7-19 (2015).
- 470 39. Semenza, G.L., Roth, P.H., Fang, H.M. & Wang, G.L. Transcriptional
471 regulation of genes encoding glycolytic enzymes by hypoxia-inducible factor
472 1. *The Journal of biological chemistry* **269**, 23757-23763 (1994).

- 473 40. Gordan, J.D., Thompson, C.B. & Simon, M.C. HIF and c-Myc: sibling rivals
474 for control of cancer cell metabolism and proliferation. *Cancer Cell* **12**, 108-
475 113 (2007).
- 476 41. Kim, J.W., Tchernyshyov, I., Semenza, G.L. & Dang, C.V. HIF-1-mediated
477 expression of pyruvate dehydrogenase kinase: a metabolic switch required for
478 cellular adaptation to hypoxia. *Cell metabolism* **3**, 177-185 (2006).
- 479 42. Papandreou, I., Cairns, R.A., Fontana, L., Lim, A.L. & Denko, N.C. HIF-1
480 mediates adaptation to hypoxia by actively downregulating mitochondrial
481 oxygen consumption. *Cell metabolism* **3**, 187-197 (2006).
- 482 43. Kluza, J. *et al.* Inactivation of the HIF-1alpha/PDK3 signaling axis drives
483 melanoma toward mitochondrial oxidative metabolism and potentiates the
484 therapeutic activity of pro-oxidants. *Cancer research* **72**, 5035-5047 (2012).
- 485 44. Atsumi, T. *et al.* High expression of inducible 6-phosphofructo-2-
486 kinase/fructose-2,6-bisphosphatase (iPFK-2; PFKFB3) in human cancers.
487 *Cancer research* **62**, 5881-5887 (2002).
- 488 45. Christofk, H.R. *et al.* The M2 splice isoform of pyruvate kinase is important
489 for cancer metabolism and tumour growth. *Nature* **452**, 230-233 (2008).
- 490 46. Wu, W. & Zhao, S. Metabolic changes in cancer: beyond the Warburg effect.
491 *Acta biochimica et biophysica Sinica* **45**, 18-26 (2013).
- 492 47. Semenza, G.L. HIF-1: upstream and downstream of cancer metabolism.
493 *Current opinion in genetics & development* **20**, 51-56 (2010).
- 494 48. de la Cova, C. *et al.* Supercompetitor status of Drosophila Myc cells requires
495 p53 as a fitness sensor to reprogram metabolism and promote viability. *Cell*
496 *metabolism* **19**, 470-483 (2014).

498

499

500 **ACKNOWLEDGEMENTS**

501 We thank K. Rajewsky for the establishment of knocked-in ES cells harbouring
502 RasV12-eGFP. We also thank H. Harada for the HIF1 reporter-expressing vector, C.
503 Kuo for the R-spondin-producing cell line and T. Yoshimori for useful advice on EM
504 analyses. Ya.F. is supported by Japan Society for the Promotion of Science (JSPS)
505 Grant-in-Aid for Scientific Research on Innovative Areas 26114001, Grant-in-Aid for
506 Scientific Research (A) 26250026 and AMED Strategic Japanese-Swiss Cooperative
507 Program. Ya.F. is also supported by the Takeda Science Foundation. Shu.K. is
508 supported by Japan Society for the Promotion of Science (JSPS) Grant-in-Aid for
509 Scientific Research on Innovative Areas 26112701, Kato Memorial Bioscience
510 Foundation and The YASUDA Medical Foundation.

511

512 **AUTHOR CONTRIBUTIONS**

513 Shu.K. designed experiments and generated most of the data. K.I. performed qRT-
514 PCR experiments and metabolic analyses. H.K. and Sho.K. designed and analysed the
515 cell competition mouse model. S.I., H.Y., Y.Y., To.Ma., H.W., Ri.E., A.N., I.K., S.T.,
516 R.N. and Ta. M. assisted experiments. M.K., A.S., Ry.E., S.H., S.Y., J.K. and M.Is.
517 performed time-lapse experiments. T.K. performed electron microscopic analyses.
518 J.M.N., Ya.O., Yo.F. and Yu.O. performed FRET analysis. H.I., To.So. and M.R.D.
519 assisted metabolic analyses. Y. S., M.O., J.M. and T.Sa. assisted *ex vivo* and *in vivo*
520 experiments. Ta.S., To.Mo., M.Im. and E.N. assisted iGT experiments. Ya.F.
521 conceived and designed the study. The manuscript was written by Shu.K. and Ya.F.
522 with assistance from the other authors.

523

524 **COMPETING FINANCIAL INTERESTS**

525 The authors declare no competing financial interests.

526

527

528 **Figure legends**

529

530 **Figure 1. Mitochondrial membrane potential is diminished in RasV12-**

531 **transformed cells that are surrounded by normal epithelial cells. (a-g)**

532 Incorporation of TMRM or mitoSOX in RasV12-transformed cells surrounded by
 533 normal cells. **(a, d, e)** Confocal images of MDCK-pTR GFP-RasV12 or MDCK-pTR
 534 GFP cells mixed with normal MDCK cells, or cultured alone. Cells were loaded with
 535 50 nM TMRM (red) **(a, b, d)** or 5 μ M MitoSOX (red) **(e, f)**. Arrows indicate RasV12-
 536 transformed cells showing diminished TMRM **(a)** or mitoSOX **(e)** fluorescence. **(b, f)**
 537 Quantification of the fluorescence intensity of TMRM **(b)** or mitoSOX **(f)**. Data are
 538 mean \pm s.e.m.. Values are expressed as a ratio relative to MDCK. * P <0.001, **unpaired**
 539 **two-tailed t-test**; n=92, 24, 53 and 60 cells **(b)** or n=52, 45 and 31 cells **(f)** **pooled**
 540 from three independent experiments. **(c)** CMTX incorporation in RasV12-
 541 transformed cells. MDCK-pTR GFP-RasV12 cells were mixed with normal MDCK
 542 cells or cultured alone, and loaded with 5 μ M CMTX (red). **(d)** Confocal images of
 543 xz sections of apically extruding or extruded RasV12-transformed cells surrounded by
 544 normal cells and of RasV12-transformed cells cultured alone. **(g)** The measurement of
 545 fluorescence intensity of TMRM or MitoSOX using image cytometer in MDCK-pTR
 546 GFP-RasV12 cells mixed with normal MDCK cells or cultured alone. Cells were
 547 loaded with 50 nM TMRM or 5 μ M MitoSOX.**(h)** Immunofluorescence images of
 548 Tom20. MDCK-pTR GFP-RasV12 cells were mixed with normal MDCK cells or
 549 cultured alone, and were stained with Hoechst 33342 (blue) and anti-Tom20 antibody
 550 (red). Scale bars, 10 μ m **(a, c-e, h)**. **Statistics source data for b, f are provided in**
 551 **Supplementary Table 2.**

552

Figure 2. Warburg effect-like metabolic changes in RasV12-transformed cells that are surrounded by normal cells. (a) 2-NBDG incorporation in myc-RasV12 cells. MDCK-pTRE3G myc-RasV12 cells co-cultured with MDCK cells or cultured alone were loaded with 100 μ M 2-NBDG. (b) Quantification of the fluorescence intensity of 2-NBDG. Data are mean \pm s.e.m.. Values are expressed as a ratio relative to MDCK. * P <0.001, unpaired two-tailed t-test; n=66, 66 and 48 cells pooled from three independent experiments. (c) Accumulation of LDHA in RasV12-transformed cells surrounded by normal cells. MDCK-pTR GFP-RasV12 cells were mixed with normal MDCK cells or cultured alone, and were stained with Hoechst 33342 (blue), anti-LDHA antibody (red) and Alexa-Fluor-647-conjugated phalloidin (white). Scale bars, 10 μ m (a, c). (d) Quantification of the percentage of LDHA-enriched RasV12-transformed cells. Data are mean \pm s.e.m.. * P <0.05, unpaired two-tailed t-test; n= two independent experiments. (e) The measurement of fluorescence intensity of LDHA using image cytometer in MDCK-pTR GFP-RasV12 cells mixed with normal MDCK cells or cultured alone. Cells were stained with Hoechst 33342 and anti-LDHA antibody. (f) Lactate concentration in the conditioned medium at 12-24 h after tetracycline addition. The mean values of the indicated single cultures are also shown as the gray bars. Data are mean \pm s.e.m.. * P <0.001, unpaired two-tailed t-test; n= five independent experiments for MDCK alone, RasV12 alone and MDCK:RasV12=1:1, two independent experiments for RasV12 shLDHA1 alone and MDCK:RasV12 shLDHA1=1:1 and three independent experiments for RasV12 shLDHA2 alone and MDCK:RasV12 shLDHA2=1:1. Statistics source data for b, d, f are provided in Supplementary Table 2.

Figure 3. PDK4 plays a crucial role in the decreased mitochondrial membrane potential and apical extrusion of RasV12-transformed cells surrounded by normal cells. (a) Quantitative RT-PCR analysis of various metabolic enzymes in RasV12-transformed cells surrounded by normal cells. MDCK-pTR GFP-RasV12 cells were co-cultured with normal MDCK cells or cultured alone. GFP-positive RasV12 cells were selectively collected by FACS sorting and subjected to qPCR analysis. Values are shown as fold change in RasV12 cells surrounded by normal cells relative to RasV12 cells cultured alone. Data are mean \pm s.e.m.. * P <0.05, unpaired two-tailed t-test; n= three or four independent experiments. (b) Immunofluorescence images of phosphorylated PDH. MDCK-pTR GFP-RasV12 were mixed with normal MDCK cells or cultured alone, and were stained with Hoechst 33342 (blue) and anti-p-PDH antibody (red). (c) Quantification of the fluorescence intensity of p-PDH. Data are mean \pm s.e.m.. Values are expressed as a ratio relative to MDCK. * P <0.005, unpaired two-tailed t-test; n=93, 147 and 89 cells pooled from three independent experiments. (d) The measurement of fluorescence intensity of p-PDH using image cytometer in MDCK-pTR GFP-RasV12 cells mixed with normal MDCK cells or cultured alone. Cells were stained with Hoechst 33342 and anti-p-PDH antibody. (e-i) Effect of PDK4-knockdown on TMRM incorporation (f, g) or apical extrusion (h, i) of RasV12 cells surrounded by normal cells. (e) Establishment of MDCK-pTR GFP-RasV12 cells stably expressing PDK4-shRNA1 or -shRNA2. Knockdown of PDK4 was confirmed by quantitative RT-PCR. Data are mean \pm s.e.m.. * P <0.01, unpaired two-tailed t-test; n= three independent experiments. (f) MDCK-pTR GFP-RasV12 PDK4-shRNA1 or -shRNA2 cells were mixed with normal MDCK cells and loaded with TMRM. (g) Quantification of the fluorescence intensity of TMRM. Data are mean \pm s.e.m.. Values are expressed as a ratio relative to MDCK. * P <0.001, unpaired

602 **two-tailed t-test**; n= 92, 92, 97 and 102 cells **pooled** from three independent
 603 experiments. **(h)** Immunofluorescence images of xz sections of MDCK-pTR GFP-
 604 RasV12 PDK4-shRNA1 or -shRNA2 cells surrounded by normal MDCK cells.
 605 Arrowheads indicate the basal protrusion. Scale bars, 10 μ m **(b, f, h)**. **(i)**
 606 Quantification of the apical extrusion and basal protrusion formation. Data are mean \pm
 607 s.e.m.. * P <0.05, **unpaired two-tailed t-test**; n=three independent experiments.
 608 **Statistics source data for a, c, e, g, i are provided in Supplementary Table 2.**

609

610 **Figure 4. DCA treatment abolishes the Warburg effect-like metabolic changes**
 611 **and suppresses apical extrusion of RasV12-transformed cells.** **(a)** Effect of DCA
 612 on p-PDH or LDHA. MDCK-pTR GFP-RasV12 cells were mixed with normal
 613 MDCK cells in the absence or presence of 25 mM DCA. Cells were stained with
 614 Hoechst 33342 (blue) and anti-p-PDH or anti-LDHA antibody (red). **(b-e)** Effect of
 615 DCA on TMRM incorporation **(b, c)** or apical extrusion **(d, e)** of RasV12-transformed
 616 cells. **(b)** MDCK-pTR GFP-RasV12 cells were co-cultured with normal MDCK cells
 617 in the absence or presence of 25 mM DCA and incubated with 50 nM TMRM. **(c)**
 618 Quantification of the fluorescence intensity of TMRM. Data are mean \pm s.e.m..
 619 Values are expressed as a ratio relative to MDCK (-DCA). * P <0.001, **unpaired two-**
 620 **tailed t-test**; n= 84, 82, 98 and 90 cells **pooled** from three independent experiments.
 621 **(d)** Immunofluorescence images of xz sections of MDCK-pTR GFP-RasV12 cells
 622 surrounded by normal MDCK cells in the absence or presence of DCA. An arrowhead
 623 indicates the basal protrusion. Scale bars, 10 μ m **(a, b, d)**. **(e)** Quantification of the
 624 apical extrusion and basal protrusion formation of RasV12 cells in the absence or
 625 presence of DCA. Data are mean \pm s.e.m.. * P <0.05, **unpaired two-tailed t-test**;

n=three independent experiments. Statistics source data for **c**, **e** are provided in
Supplementary Table 2.

628

Figure 5. EDAC and EPLIN act upstream of the Warburg effect-like metabolic changes in RasV12 cells surrounded by normal cells. (a) TMRM incorporation in EPLIN-knockdown RasV12-transformed cells. MDCK-pTR GFP-RasV12 cells or MDCK-pTR GFP-RasV12 EPLIN-shRNA1 cells were co-cultured with normal MDCK cells and loaded with 50 nM TMRM. (b) Quantification of the fluorescence intensity of TMRM. Data are mean \pm s.e.m.. Values are expressed as a ratio relative to MDCK. * $P < 0.001$, unpaired two-tailed t-test; n=64, 21 and 45 cells pooled from two independent experiments. (c) Effect of EPLIN-knockdown on the mRNA level of PDK4 in RasV12 cells surrounded by normal cells. MDCK-pTR GFP-RasV12 cells or MDCK-pTR GFP-RasV12 EPLIN-shRNA1 cells were co-cultured with normal MDCK cells or cultured alone. GFP-positive RasV12 cells were selectively collected by FACS sorting and subjected to qPCR analysis. Values are shown as fold change in RasV12 cells surrounded by normal cells relative to RasV12 cells cultured alone. Data are mean \pm s.e.m.. * $P < 0.05$, unpaired two-tailed t-test; n= three independent experiments. (d) Effect of EPLIN-knockdown on PDH phosphorylation or LDHA accumulation. MDCK-pTR GFP-RasV12 cells or MDCK-pTR GFP-RasV12 EPLIN-shRNA1 cells were co-cultured with normal MDCK cells. Cells were stained with Hoechst 33342 (blue) and anti-p-PDH or anti-LDHA antibody (red). (e) TMRM incorporation in RasV12-transformed cells surrounded by Filamin-knockdown cells. MDCK-pTR GFP-RasV12 cells were co-cultured with MDCK cells or MDCK-pTR Filamin-shRNA1 cells, and loaded with 50 nM TMRM. (f) Quantification of the fluorescence intensity of TMRM. Data are mean \pm s.e.m.. Values are expressed as a

ratio relative to MDCK. * $P < 0.001$, unpaired two-tailed t-test; $n = 50, 41$ and 42 cells
pooled from three independent experiments. (g) Effect of Filamin-knockdown in the
surrounding normal cells on PDH phosphorylation or LDHA accumulation in
RasV12-transformed cells. MDCK-pTR GFP-RasV12 cells were co-cultured with
MDCK-pTR Filamin-shRNA1 cells. Cells were stained with Hoechst 33342 (blue)
and anti-p-PDH or anti-LDHA antibody (red). Scale bars, $10\ \mu\text{m}$ (a, d, e, g). Statistics
source data for b, c, f are provided in Supplementary Table 2.

Figure 6. FRET analyses for intracellular glucose. (a) Schematics for Glucose-
FRET. (b) Glucose-FRET images. MDCK-pTRE3G myc-RasV12 cell lines stably
expressing FLII¹²Pglu-700 $\mu\delta$ 6 (RasV12 Glu-FRET No. 1 or No. 2) were co-cultured
with MDCK cells or cultured alone with doxycycline for 16 h and then analysed by
dual-emission fluorescence microscopy. FRET/CFP ratio images were generated to
represent FRET efficiency. Scale bars, $10\ \mu\text{m}$. (c) Quantification of Glucose-FRET
efficiency (FRET/CFP). The box plots represent values from the 25th (bottom) to the
75th (top) percentiles, with the median as the horizontal line. * $P < 0.001$, unpaired two-
tailed t-test; $n = 40, 61, 41$ and 68 cells pooled from three independent experiments.
Statistics source data for c are provided in Supplementary Table 2.

Figure 7. PDK-mediated mitochondrial dysfunction induces apical elimination of
RasV12-transformed cells ex vivo. (a) Strategy for the establishment of the cell
competition mouse model. (b) Immunofluorescence images of intestinal organoids
from Villin-Cre^{ERT2};LSL-RasV12-IRES-eGFP or ;LSL-eGFP mice after treatment of
100 nM tamoxifen. The areas in the white boxes are shown at higher magnification in
the lower panels. ‘Extruding’; with their nucleus apically shifted, but still attached to

676 the basement membrane. 'Extruded'; completely detached from the basement
 677 membrane and translocated into the apical lumen. Data are mean \pm s.e.m.. * P <0.001
 678 for extruded + extruding between RasV12-GFP- and GFP-expressing cells, **unpaired**
 679 **two-tailed t-test; n=three independent experiments.** (c) Immunofluorescence images
 680 of intestinal organoids from *villin-Cre^{ERT2};LSL-RasV12-IRES-eGFP* mice at 24 h after
 681 1 μ M tamoxifen treatment. The arrow and arrowhead indicate an apically extruding
 682 RasV12 cell and the cluster of several RasV12 cells that are not extruded and remain
 683 within the epithelium, respectively. For quantification, the clusters are categorized by
 684 the number of RasV12 cells present in each cluster. Data are mean \pm s.e.m.. **n=three**
 685 **independent experiments.** (d-f) TMRM incorporation (d, e) or immunofluorescence of
 686 p-PDH (f) in intestinal organoids from *villin-Cre^{ERT2};LSL-RasV12-IRES-eGFP* or
 687 *;LSL-eGFP* mice at 24 h after tamoxifen treatment. Arrows indicate RasV12-
 688 transformed cells with elevated PDH phosphorylation. (e) Quantification of the
 689 fluorescence intensity of TMRM. Data are mean \pm s.e.m.. * P <0.001, **unpaired two-**
 690 **tailed t-test; n=71, 37, 30 and 28 cells pooled** from three independent experiments. (g,
 691 h) Effect of DCA on apical extrusion *ex vivo*. (g) Intestinal organoids from *villin-*
 692 *Cre^{ERT2};LSL-RasV12-IRES-eGFP* mice were treated with 100 nM tamoxifen and
 693 cultured for 24 h in the absence or presence of DCA. Asterisks in the images indicate
 694 mucin-rich, autofluorescent materials in the apical lumen (b-d, f, g). Ba and Ap stand
 695 for the basal and apical side, respectively (b-d, f, g). Scale bars, 10 μ m (b-d, f, g). (h)
 696 Quantification of the effect of DCA on apical extrusion *ex vivo*. Data are mean \pm
 697 s.e.m.. * P <0.005, **unpaired two-tailed t-test; n=two or three independent experiments.**
 698 **Statistics source data for b, c, e, h are provided in Supplementary Table 2.**
 699

Figure 8. PDK-mediated mitochondrial dysfunction induces apical elimination of RasV12-transformed cells *in vivo*. (a) Immunofluorescence images of intestinal villi from *Villin-Cre^{ERT2};LSL-eGFP* or *;LSL-RasV12-IRES-eGFP* mice after tamoxifen injection. Note that apicobasal polarity is **apparently reversed** between *ex vivo* and *in vivo*. (b) ‘Not extruded’; remaining within the epithelium. ‘Apical extruding’; with their nucleus apically shifted, but still attached to the basement membrane. ‘Apical extruded’; completely detached from the basement membrane and translocated into the apical lumen. An arrow indicates ‘Basal extruding’; basally delaminated beneath the basement membrane. (c) Quantification of the apical and basal extrusion. Data are mean \pm s.e.m.. * $P < 0.05$ for extruded + extruding between GFP- and RasV12-GFP-expressing cells, **unpaired two-tailed t-test; n=two independent experiments**. (d) Intravital two-photon imaging of the small intestine of *Villin-Cre^{ERT2};LSL-RasV12-IRES-eGFP* mice. The arrowhead indicates an apically extruding cell. Scale bar, 50 μ m. (e) *villin-Cre^{ERT2};LSL-RasV12-IRES-eGFP* or *;LSL-eGFP* mice pre-treated with or without DCA were injected with tamoxifen and sacrificed 3 days later while DCA was continuously administrated during this period. Arrowheads indicate apically extruding or extruded cells. (f) Quantification of the effect of DCA on apical extrusion *in vivo*. Data are mean \pm s.e.m.. * $P < 0.01$, **unpaired two-tailed t-test; n=two or three independent experiments**. (g) An iGT operated mouse. The dotted line indicates the iGT-operated intestinal region. (h) Immunofluorescence images of iGT-operated intestinal villi with or without Cy3-siRNA-containing HVJ-E. Scale bars, 100 μ m. (i) Effect of scramble- or PDK4-siRNA on expression of PDK4 in the iGT-operated intestinal epithelium. PDK4-knockdown is confirmed by western blotting. (j) Immunofluorescence images of intestinal villi from the non iGT-operated region and scramble- or PDK4-siRNA transfected region at 3 days after tamoxifen injection.

725 Arrows indicate apically extruding or extruded cells. Scale bars, 10 μm (**a**, **b**, **e**, **j**). (**k**)

726 Quantification of the apical and basal extrusion of RasV12-transformed cells. Data are

727 mean \pm s.e.m.. * $P < 0.01$, unpaired two-tailed t-test; n= three independent experiments.

728 For Fig. 8i, an unprocessed original scan of immunoblotting is also shown in

729 Supplementary Fig. 9. Statistics source data for **c**, **f**, **k** are provided in Supplementary

730 Table 2.

731

732

1 **METHODS**

2 **Antibodies, plasmids and materials**

3 The following antibodies were used in this study; goat anti-LDHA (sc-27230), mouse
4 anti-Tom20 (sc-17764 clone F10) and mouse anti-EPLIN (sc-136399 clone 20)
5 antibodies from Santa Cruz Biotechnology, mouse anti-myc (05-724 clone 4A6) and
6 mouse anti- β -actin (MAB1501R clone C4) antibodies from Millipore, rabbit
7 anti-phospho-PDH antibody (AP1062) from Calbiochem, mouse anti-PDH (ab110330
8 clone 9H9AF5) and chicken anti-GFP (ab13970) antibodies from Abcam, mouse
9 anti-E-cadherin antibody (610181 clone 36) from BD Transduction and rabbit
10 anti-PDK4 antibody (AP7041B) from ABGENT. Alexa-Fluor-568- and
11 -647-conjugated phalloidin (Life Technologies) were used at 1.0 U ml^{-1} .
12 Alexa-Fluor-568- and -647-conjugated secondary antibodies were from Life
13 Technologies. Hoechst 33342 (Life Technologies) was used at a dilution of 1:5,000.
14 TMRM, mitoSOX, MitoTracker Green and 2-NBDG
15 (2-deoxy-2-[(7-nitro-2,1,3-benzoxadiazol-4-yl)amino]-D-glucose) were obtained from
16 Molecular Probes. The following inhibitors, Radicol ($10 \mu\text{M}$), (S)-(-)-blebbistatin

17 (30 μ M), KT5720 (4 μ M), 3-MA (10 mM), Y27632 (20 μ M) and Chrysin (100 μ M)
18 were from Calbiochem. L-NAME (300 μ M) was from Santa Cruz, and Cytochalasin D
19 (4 μ M), NAC (5 mM), 2-DG (25 mM) and DCA (25 mM except for Fig. 7g, h and
20 Supplementary Fig. 7c, d where 50 mM was used) were from Sigma-Aldrich.

21

22 **Cell culture**

23 MDCK cell lines were used in this study. Parental MDCK cell is the gift from Walter
24 Birchmeier. The cell line was not found in the database of commonly misidentified cell
25 lines that is maintained by ICLAC and NCBI Biosample. Mycoplasma contamination is
26 regularly tested for all cell lines in use using a commercially available kit (MycoAlert,
27 Lonza). The cell lines were not further authenticated. MDCK, MDCK-pTR
28 GFP-RasV12, MDCK-pTR cSrcY527F-GFP, MDCK-pTR Scribble-shRNA,
29 MDCK-pTR GFP-RasV12 EPLIN-shRNA and MDCK-pTR Filamin A-shRNA cells
30 were cultured as previously described^{10, 14-16}. To establish MDCK -pTRE3G
31 myc-RasV12 cells, cDNA of myc-H-RasV12 was cloned into BamHI/EcoRI sites of
32 pPB-TRE3G-MCS-CEH-rtTA3-IP, which was constructed by introducing the TRE3G

33 promoter with cloning sites, insulator and rtTA3-expressing elements into a
34 PiggyBac-based vector (SBI). MDCK cells were then transfected with pPB-TRE3G
35 myc-RasV12 by nucleofection (nucleofector 2b Kit L, Lonza), followed by selection in
36 medium containing 5 $\mu\text{g ml}^{-1}$ blasticidin (Invitrogen). MDCK-pTRE3G myc-RasV12
37 cells stably expressing FLII¹²Pglu-700 $\mu\delta 6$ ⁴⁹ were established by co-transfecting MDCK
38 cells with pPB-TRE3G myc-RasV12 and pPB-FLII¹²Pglu-700 $\mu\delta 6$, followed by the
39 same selection method as above. To establish MDCK-pTR GFP-RasV12 cells stably
40 expressing PDK4-shRNA, LDHA-shRNA or Luciferase-shRNA, or MDCK cells stably
41 expressing PDH-shRNA or Luciferase-shRNA in a tetracycline-inducible manner, each
42 shRNA sequences were cloned into the *BglII* and *XhoI* site of pSUPER.neo+gfp (for the
43 former three shRNAs) or pSUPERIOR.neo+gfp (for the latter two
44 shRNAs)(Oligoengine). Sequences of shRNAs are listed in Supplementary Table 1. For
45 tetracycline-inducible MDCK cell lines, 2 $\mu\text{g ml}^{-1}$ of tetracycline (Sigma-Aldrich) was
46 used to induce expression of proteins or shRNAs except for MDCK-pTRE3G
47 myc-RasV12 cells for which 1 $\mu\text{g ml}^{-1}$ of doxycycline (Sigma-Aldrich) was used.
48 MDCK-pTR Filamin A-shRNA cells were incubated with tetracycline for 48 h to

49 induce sufficient knockdown prior to co-incubation with MDCK-pTR GFP-RasV12
50 cells. For immunofluorescence, cells were plated onto collagen gel-coated coverslips.
51 Type-I collagen (Cellmatrix Type I-A) was obtained from Nitta Gelatin and was
52 neutralized on ice to a final concentration of 2 mg ml^{-1} according to the manufacturer's
53 instructions. The CellTracker dyes, CMTPX (red dye), CMFDA (green dye) and
54 CMAC (blue dye) (Life Technologies) were used according to the manufacturer's
55 instructions.

56

57 **CRISPR/Cas9-based generation of PDK4 knockout cells**

58 Guide sequences of PDK4 sgRNA1 and 2 targeting canine *PDK4* were designed on the
59 exon 1 and 9, respectively, as described previously⁵⁰. PDK4 sgRNA sequences (PDK4
60 sgRNA1, 5'-GCTTCGTGATGCGCAGCGC-3'; PDK4 sgRNA2,
61 5'-ACGGCACCAACGCCTGTGA-3') were introduced into the
62 pCDH-EF1-Hygro-sgRNA vector⁵¹ using primers listed in Supplementary Table 1.
63 First, MDCK cells were infected with lentivirus carrying pCW-Cas9 as described⁵¹, and
64 were cultured in the 500 ng ml^{-1} puromycin-containing medium. The

tetracycline-inducible MDCK-Cas9 cells were transfected with the pCDH-EF1-PDK4 sgRNA1 and 2 by nucleofection, followed by selection in medium containing 200 μ g ml⁻¹ of Hygromycin and subjected to limiting dilution. Indels on the *PDK4* exons in each monoclonal were analysed by direct sequencing using primers listed in Supplementary Table 1. To generate PDK4-deleted cells carrying doxycycline-inducible GFP-RasV12, pPB-TRE3G GFP-RasV12 was introduced into the PDK4-deleted cells by nucleofection and antibiotics selection. In addition to the PDK4^{-/-} MDCK-pTRE3G GFP-RasV12 cells, we generated PDK4^{+/+} MDCK-pTRE3G GFP-RasV12 cells as a control cell line.

74

75 Mice

All animal experiments were conducted under the guidelines by the Animal Care Committee of Hokkaido University. The animal protocols were reviewed and approved by the Hokkaido University Animal Care Committee (Approval number:12-0116). We used 6-10 weeks old C57BL/6 mice of either sex. To establish *DNMT1*-CAG-*loxP*-STOP-*loxP*-HRas^{V12}-IRES-eGFP knock-in mice, the genomic

81 fragments of DNA methyltransferase 1 (DNMT1) locus, the *loxP*-flanked stop and
82 *neomycin resistance* cassette, cDNA encoding HRas^{V12} plus *frt*-flanked IRES-eGFP and
83 *diphtheria toxin subunit A* gene were inserted into the targeting vector. The resulting
84 plasmid DNA was linearized and electrophoretically transfected into IB10 ES cells.
85 Recombinant alleles were verified by Southern blot analysis. The independent clones
86 were each injected into blastocysts of C57BL/6 mice and were successfully transmitted
87 through the germ-line, and *DNMT1-CAG-loxP-STOP-loxP-HRas^{V12}-IRES-eGFP* mice
88 (acc. no. CDB0706K: <http://www2.clst.riken.jp/arg/mutant%20mice%20list.html>) were
89 thus established. *Villin-Cre^{ERT2}* mice⁵² were crossed with
90 *DNMT1-CAG-loxP-STOP-loxP-HRas^{V12}-IRES-eGFP* mice or
91 *CAG-loxP-STOP-loxP-eGFP* mice⁵³ to create Villin-RasV12-GFP or Villin-GFP mice
92 respectively. Mice heterozygous for each transgene were used for experiments. For PCR
93 genotyping of mice, primers listed in Supplementary Table 1 were used. The expected
94 sizes of PCR products were 220 bp, 403 bp and 390 bp for *Villin-Cre^{ERT2}*,
95 *DNMT1-CAG-loxP-STOP-loxP-HRas^{V12}-IRES-eGFP* and
96 *CAG-loxP-STOP-loxP-eGFP* mice, respectively. For culturing intestinal organoids,

97 isolated crypts from the mouse small intestine were entrapped in Matrigel (Corning) and
98 plated in a non-coated 35-mm glass bottom dish as previously described³⁶. The crypts
99 embedded in Matrigel were covered with Advanced DMEM/F12 supplemented with N2
100 (Invitrogen), B27 (Invitrogen), 50 ng ml⁻¹ EGF (Peprotech), 100 ng ml⁻¹ Noggin
101 (Peprotech), 1.25 mM N-Acetylcystein (Sigma-Aldrich) and R-spondin conditioned
102 medium collected from 293T-HA-Rspol-Fc cells kindly provided by Dr. Calvin Kuo
103 (Stanford University). After 96 h culture, organoids were incubated with tamoxifen
104 (Sigma) for 24 h to induce transgenes. Subsequently, tamoxifen was washed out, and
105 organoids were cultured for the indicated times for analyses. For *in vivo* experiments,
106 6-10 weeks old Villin-RasV12-GFP or Villin-GFP mice were given a single
107 intraperitoneal injection of 2 mg of tamoxifen in corn oil (Sigma), and were then
108 sacrificed at 2, 3, 5 or 7 days after Cre activation. To examine the effect of DCA, the
109 mice were first pretreated with 5.0 g l⁻¹ DCA in the drinking water for 2 weeks.
110 Subsequently, the mice were injected intraperitoneally with 2.0 mg of tamoxifen and
111 sacrificed 3 days later while DCA was continuously administrated during this period.
112 The iGT (intestine-specific gene transfer) experiments were performed as previously

113 described³⁷. Briefly, 3-5 cm regions of small intestine drawn out from the peritoneal
114 cavity were tied with nylon string. 300 µl of the mucus removing solution (20 mM
115 DTT, 0.05% Tween-20 in PBS) was injected into the intestinal lumen for 15 min,
116 removed and incubated with the same solution for 10 min. After washing with PBS
117 three times by pipetting, 300 µl of the transfection solution containing Cy3-labelled
118 siRNA and HVJ-E (haemagglutinating virus of Japan envelope) was injected, and the
119 mice were left for 1 h. The sequences of Scramble- and PDK4-siRNA are listed in
120 Supplementary Table 1. 2.0 mg of tamoxifen was injected into the peritoneal cavity
121 when the wound was sutured. The mice were sacrificed for the analysis after 3 days of
122 iGT.

123

124 **Immunofluorescence and western blotting**

125 For immunofluorescence, MDCK-pTR GFP-RasV12, MDCK-pTR cSrcY527F-GFP,
126 MDCK-pTR Scribble-shRNA, MDCK-pTRE3G myc-RasV12, MDCK-pTR
127 GFP-RasV12 PDK4-shRNA, MDCK-pTRE3G GFP-RasV12 PDK4-sgRNA,
128 MDCK-pTR PDH-shRNA, MDCK-pTR GFP-RasV12 EPLIN-shRNA, MDCK-pTR

129 GFP-RasV12 LDHA-shRNA or MDCK-pTR GFP-RasV12 Luciferase-shRNA cells
130 were mixed with MDCK, MDCK-pTR Filamin A-shRNA or MDCK-pTR
131 Luciferase-shRNA cells at a ratio of 1:50 and plated onto collagen-coated coverslips as
132 previously described¹⁰. The mixture of cells was incubated for 8-12 h, followed by
133 tetracycline or doxycycline treatment for 16 h, except for analyses of apical extrusions
134 that were examined after 24 h of tetracycline or doxycycline addition. Cells were fixed
135 with 4% paraformaldehyde (PFA) in PBS and permeabilised as previously described¹¹.
136 All primary antibodies were used at 1:100, and all secondary antibodies were used at
137 1:200. To monitor the mitochondrial activity or superoxide production, cells were
138 loaded with 50 nM TMRM or 5 μ M MitoSOX respectively for 30 min and subjected to
139 microscopic observation or quantitatively analysed by CellInsightTM image cytometer
140 (Thermo Fisher Scientific). As to TMRM, we have thoroughly checked and optimized
141 the experimental conditions. After titration of TMRM concentration, we chose 50 nM
142 that provides clear and sufficient fluorescence intensity. By checking the effect of
143 oligomycin and FCCP, we confirmed that the experimental condition is under the
144 non-quenching mode using 50 nM TMRM⁵⁴. We also confirmed that 2 μ g ml⁻¹

145 tetracycline did not affect TMRM fluorescence. The ratiometric images of TMRM and
146 MitoTracker Green were obtained by incubating cells with 200 nM MitoTracker Green
147 for 2 h, briefly washed, and then loaded with 50 nM TMRM. The 2-NBDG uptake was
148 examined by incubating cells with glucose-free DMEM for 2 h followed by addition of
149 100 μ M 2-NBDG for 30 min. For immunofluorescence using intestinal organoids, cells
150 grown in matrigels were incubated with Cell Recovery Solution (Corning) for 8 min
151 before fixation with 4% PFA. After fixation, cells were permeabilised in 0.5% Triton
152 X-100/PBS for 1 h and blocked in 1% BSA/PBS for 1 h. For immunohistochemical
153 examinations of the small intestine, the tissues were isolated and fixed in 4% PFA,
154 dehydrated, and embedded in paraffin. Microsections of each specimen were placed on
155 glass slides, de-paraffinized and processed for immunostaining. The iGT-operated small
156 intestine was embedded in OCT compound (Tissue-Tek), and frozen sections (10 μ m)
157 were cut on a cryostat. Immunofluorescence images were analysed by the Olympus
158 FV1000 or FV1200 system and Olympus FV10-ASW software. Images were quantified
159 by the MetaMorph software (Molecular Devices). Western blotting was performed as

160 previously described⁵⁵. Primary antibodies were used at 1:1,000. The western blotting
161 data were analysed using ImageQuantTM LAS4010 (GE Healthcare).

162

163 **FRET analysis**

164 Glucose-FRET experiments were performed as previously described⁵⁶. In brief,
165 MDCK-pTRE3G myc-RasV12 cells stably expressing FLII¹²Pglu-700 μ δ 6 were
166 co-cultured with MDCK cells at a ratio of 1:50 or cultured alone on a collagen gel in
167 35-mm-diameter, glass-bottom dishes (Matsunami Glass). At 16 h after doxycycline
168 addition, a differential interference contrast (DIC) image and CFP and FRET
169 fluorescence images were recorded. FRET efficiency was calculated as a quotient of
170 background-subtracted FRET and CFP images and is presented in an intensity-modified
171 display mode with the MetaMorph software. In the intensity-modified display mode,
172 eight colors from red to blue are used to represent the FRET efficiency. To evaluate
173 ATP level, MDCK-pTRE3G myc-RasV12 cells were transiently transfected with
174 ATeam probe⁵⁷, stained with CMTX, and were co-cultured with MDCK cells at ratio

175 of 1:50 or cultured alone on a collagen gel in 35-mm-diameter, glass-bottom dishes. At

176 16 h after doxycycline addition, FRET efficiency was examined as described above.

177

178 **Time-lapse microscopic observation**

179 For *ex vivo* time-lapse analyses, intestinal organoids grown in matrigels were incubated

180 with 100 nM tamoxifen for 24 h to induce transgenes. Subsequently, time-lapse

181 observation was carried out for 24 h in the medium containing no tamoxifen by the

182 Nipkow spinning disk confocal microscopy (X-Light; Crest Optics). Fluorescence

183 images (853 x 720 pixels, 0.975- μ m resolution) were captured at an exposure of 0.25 s.

184 Images of 42- μ m depth in the z-axis were obtained at 3- μ m z-steps.

185 For intravital imaging of small intestine in living mice, mice were anesthetized with

186 isoflurane, the small intestine was surgically exposed, and then villi were observed by

187 using two-photon excitation microscopy. Intestinal lumen was visualized with 70-kDa

188 tetramethylrhodamine-conjugated dextran (Sigma). Nuclei of cells were stained with

189 intravenous injection of Hoechst33342 (Life Technologies) just before imaging. The

190 imaging system was composed of a two-photon microscope (A1-MP; Nikon) driven by

191 a laser (Chameleon Vision II Ti: Sapphire; Coherent) tuned to 880 nm and an inverted
192 microscope equipped with a 20× objective lens (Plan Fluor; N.A., 0.75; Nikon).
193 Fluorescent signals were detected through band-pass emission filters at 525/50 nm (for
194 GFP) and at 575/25 nm (for tetramethylrhodamine). Raw imaging data were processed
195 using the Imaris software (Bitplane).

196

197 **Electron microscopy**

198 MDCK-pTR GFP-RasV12 cells were cultured alone or co-cultured with MDCK cells in
199 collagen gel-coated, grid-imprinted plastic dishes (μ -Dish 35-mm Grid-500, Ibidi
200 Corporation). After tetracycline treatment for 24 h, cells were fixed in 2%
201 glutaraldehyde in HEPES buffer (30 mM HEPES, 0.1 M NaCl and 2 mM CaCl_2 (pH
202 7.4)), and fluorescence and DIC images of GFP-RasV12 cells and the surrounding cells
203 were captured together with the underlying, numbered grid information. Cells were then
204 post-fixed in 2% osmium tetroxide in 0.1 M imidazole (pH 7.4) and stained with 1%
205 uranyl acetate (UA) before being dehydrated and embedded in Araldite-Epon resin
206 (Electron Microscopy Sciences). During these procedures, GFP fluorescence was lost,

207 but the grid was imprinted onto the resin. Subsequently, GFP-RasV12 cells and the 2 or
208 3 rows of surrounding MDCK cells were selected and excised, while referring to the
209 grid information, morphology of the cells and the captured images. Ultrathin sections of
210 the trimmed sample were poststained with UA and lead citrate, and cells were imaged
211 with an electron microscope (JEM-1400; JEOL Corporation) operating at 80 kV.

212

213 **Quantitative real-time PCR**

214 MDCK-pTR GFP-RasV12 cells or 10:1 mix culture of MDCK and MDCK-pTR
215 GFP-RasV12 cells were cultured at a density of 2×10^7 cells on the collagen-coated
216 15-cm dishes (Greiner-Bio-One). After incubation with tetracycline for 16 h,
217 GFP-positive RasV12 cells and GFP-negative MDCK cells were separated with an
218 analytical flow cytometer. Total RNA was extracted from the isolated cells using
219 Trizol® (Thermo Fisher Scientific) and the RNeasy Mini Kit (QIAGEN) and reverse
220 transcribed using QuantiTect Reverse Transcription Kit (QIAGEN). GeneAce SYBR
221 qPCR Mix (NIPPON GENE) was used to perform qPCR using the StepOne™ system

222 (Thermo Fisher Scientific). The primer sequences used are listed in Supplementary

223 Table 1. We used β -actin as a reference gene to normalise data.

224

225 **Lactate assay**

226 For lactate assay, MDCK cells, MDCK-pTR GFP-RasV12 cells, MDCK-pTR

227 GFP-RasV12 LDHA-shRNA cells or 1:1 mix of MDCK and MDCK-pTR GFP-RasV12

228 or MDCK-pTR GFP-RasV12 LDHA-shRNA cells were cultured at a density of 6.5×10^5

229 cells on the collagen-coated 12-well dishes (Falcon) in DMEM containing neither

230 phenol red nor fetal calf serum. The culture medium was replaced with fresh medium at

231 12 h after tetracycline addition and collected 12 h later. Samples were subjected to

232 measurement of lactate concentration using Lactate Assay kit (BioVision).

233

234 **HIF1 reporter assay**

235 MDCK or MDCK-pTR GFP-RasV12 cells were co-transfected with pCDH/5HRE-Luc

236 (kindly provided by Dr. Hiroshi Harada (Kyoto University)) and pRL-TK. After 24 h,

237 cells were trypsinised, and cultured alone or co-cultured with the indicated cells (total

238 cell number: 3.5×10^5) for 8 h, followed by tetracycline treatment for 16 h. Firefly
239 luciferase activity was measured using Dual-Luciferase Reporter assay (Promega) and
240 normalized by Renilla luciferase activity.

241

242 **Statistics and reproducibility**

243 For data analyses, unpaired two-tailed Student's *t*-tests were used to determine
244 *P*-values. *P*-values less than 0.05 were considered to be significant. No statistical
245 method was used to predetermine sample size. For animal studies, the experiments were
246 not randomized, and the investigators were not blinded to allocation during
247 experiments. All results were reproduced with at least two independent experiments and
248 at least three mice of each genotype. Representative figures are shown in Fig. 1c, g, h,
249 2e, 3d, 4a, 5d, g, 7f, 8d, h, i and Supplementary Fig. 1a-c, f, 3c-j, 4a, d, e, h-j, 5a-c, 6b,
250 7a, b. Each experiment was repeated independently: 2 repeats (Fig. 1c, g, 2e, 3d, 8h, i
251 and supplementary Fig. 1c, f, 3d, i, 4a, d, e, h, j, 5a, b, 7b.), 3 repeats (Fig. 1h, 4a, 5d, g,
252 8d and supplementary Fig. 1a, b, 3c, e, f, h, j 4i, 5c, 7a.), 4 repeats (Fig. 7f and

253 supplementary Fig. 3g). The experiment of supplementary Fig. 6b was performed once,
 254 but homologous recombination in ES cells was confirmed by PCR.

255

256 **Data availability**

257 Source data for Fig. 1b, f, 2b, d, f, 3a, c, e, g, i, 4c, e, 5b, c, f, 6c, 7b, c, e, h, 8c, f, k and

258 Supplementary Fig. 1e, h, 3l, n, 4c, g, 5f, g, i, 6c, 7d, e have been provided as

259 Supplementary Table 2. All data supporting the findings of this study are available from
 260 the corresponding author on request.

261

262 **Reference for Methods**

- 263 49. Hou, B.H. *et al.* Optical sensors for monitoring dynamic changes of intracellular
 264 metabolite levels in mammalian cells. *Nature protocols* **6**, 1818-1833 (2011).
- 265 50. Hsu, P.D. *et al.* DNA targeting specificity of RNA-guided Cas9 nucleases. *Nat*
 266 *Biotechnol* **31**, 827-832 (2013).
- 267 51. Maruyama, T. *et al.* Corrigendum: Increasing the efficiency of precise genome
 268 editing with CRISPR-Cas9 by inhibition of nonhomologous end joining. *Nat*
 269 *Biotechnol* **34**, 210 (2016).
- 270 52. el Marjou, F. *et al.* Tissue-specific and inducible Cre-mediated recombination in
 271 the gut epithelium. *Genesis* **39**, 186-193 (2004).
- 272 53. Kawamoto, S. *et al.* A novel reporter mouse strain that expresses enhanced green
 273 fluorescent protein upon Cre-mediated recombination. *FEBS letters* **470**, 263-268
 274 (2000).
- 275 54. Perry, S.W., Norman, J.P., Barbieri, J., Brown, E.B. & Gelbard, H.A.
 276 Mitochondrial membrane potential probes and the proton gradient: a practical
 277 usage guide. *BioTechniques* **50**, 98-115 (2011).

- 278 55. Hogan, C. *et al.* Rap1 regulates the formation of E-cadherin-based cell-cell
279 contacts. *Mol Cell Biol* **24**, 6690-6700 (2004).
- 280 56. Yamamoto, S. *et al.* A role of the sphingosine-1-phosphate (S1P)-S1P receptor 2
281 pathway in epithelial defense against cancer (EDAC). *Mol Biol Cell* **27**, 491-499
282 (2016).
- 283 57. Imamura, H. *et al.* Visualization of ATP levels inside single living cells with
284 fluorescence resonance energy transfer-based genetically encoded indicators.
285 *Proc Natl Acad Sci U S A* **106**, 15651-15656 (2009).

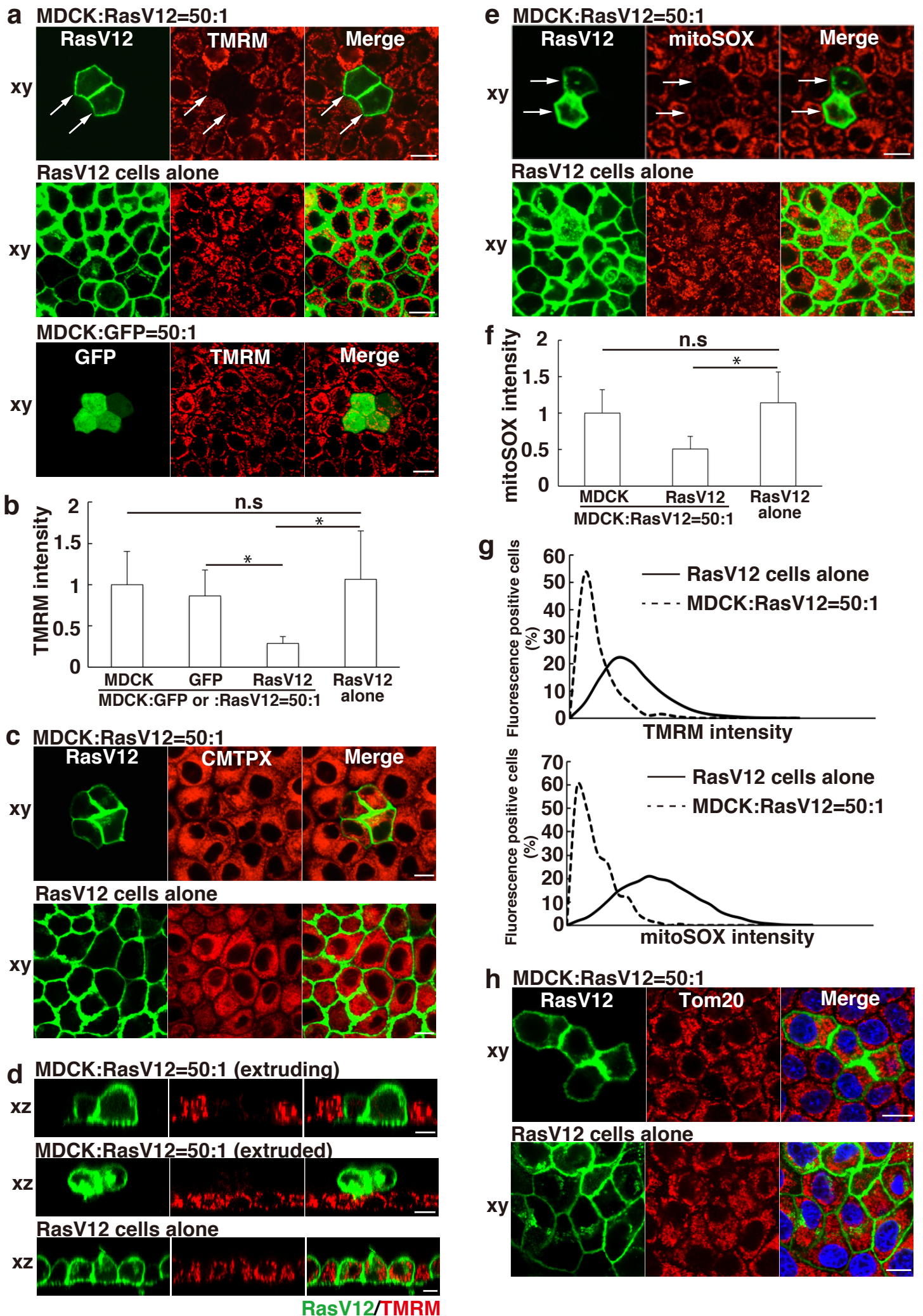


Figure 1 Kon et al.

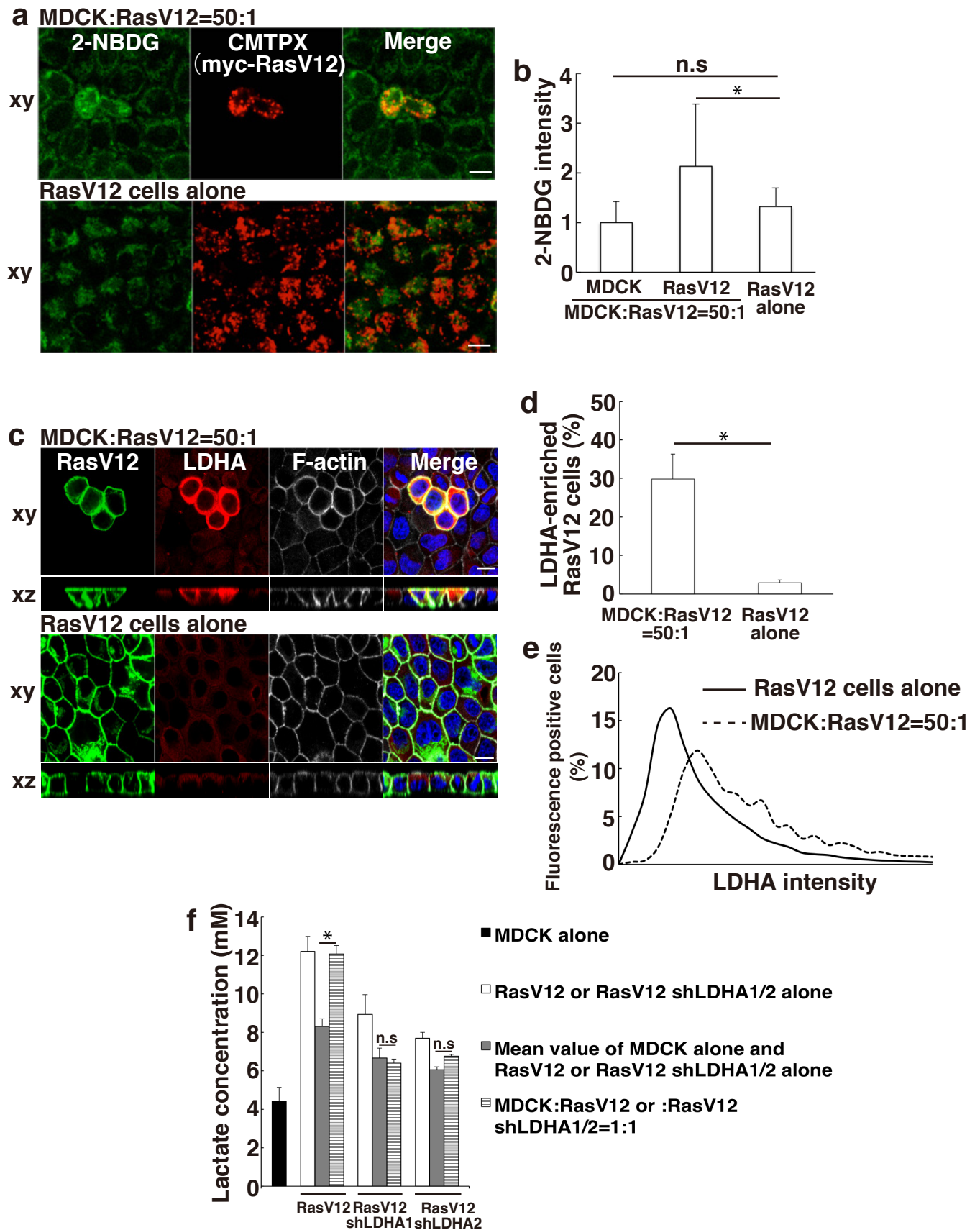


Figure 2 Kon et al.

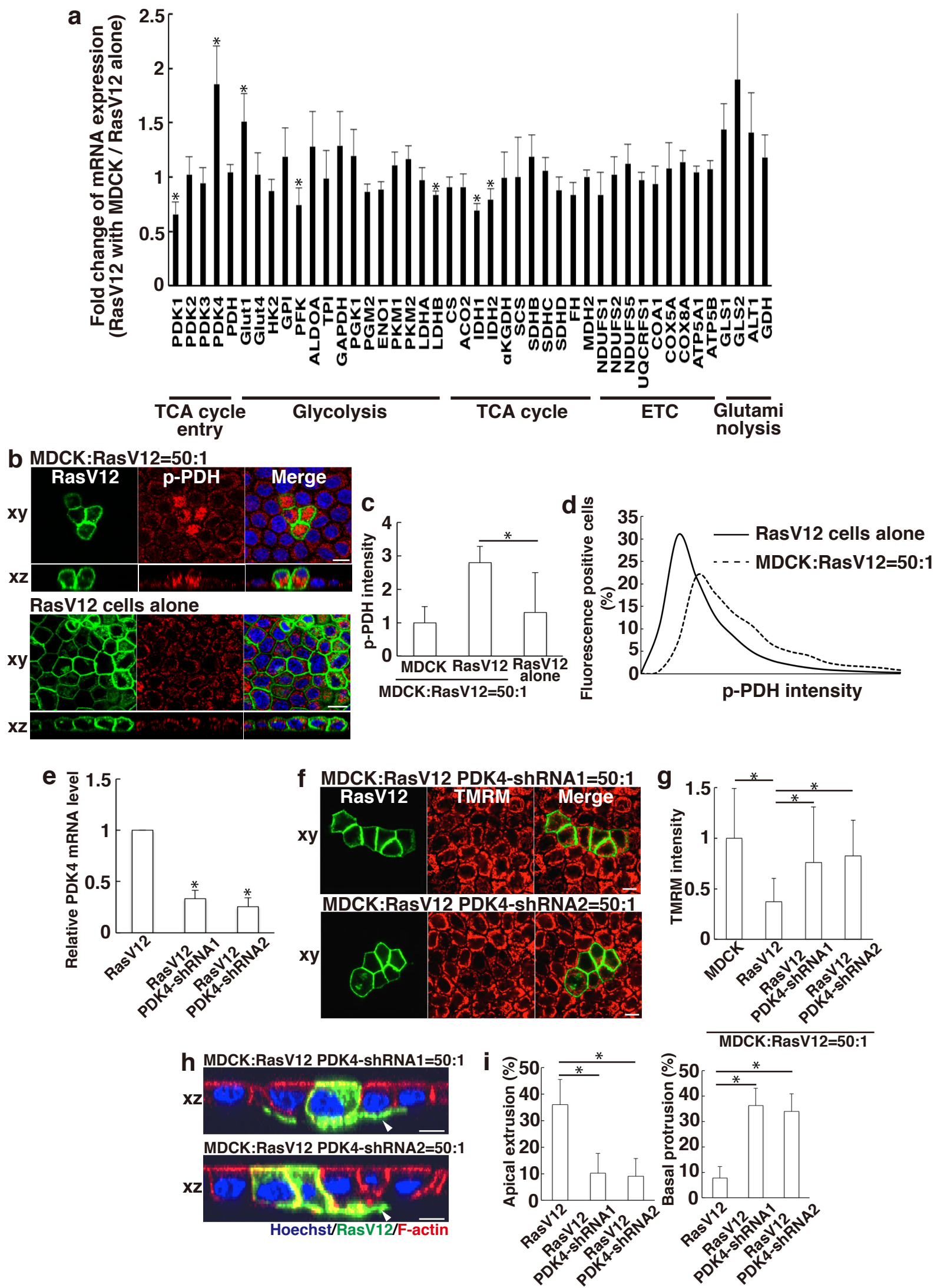


Figure 3 Kon et al.

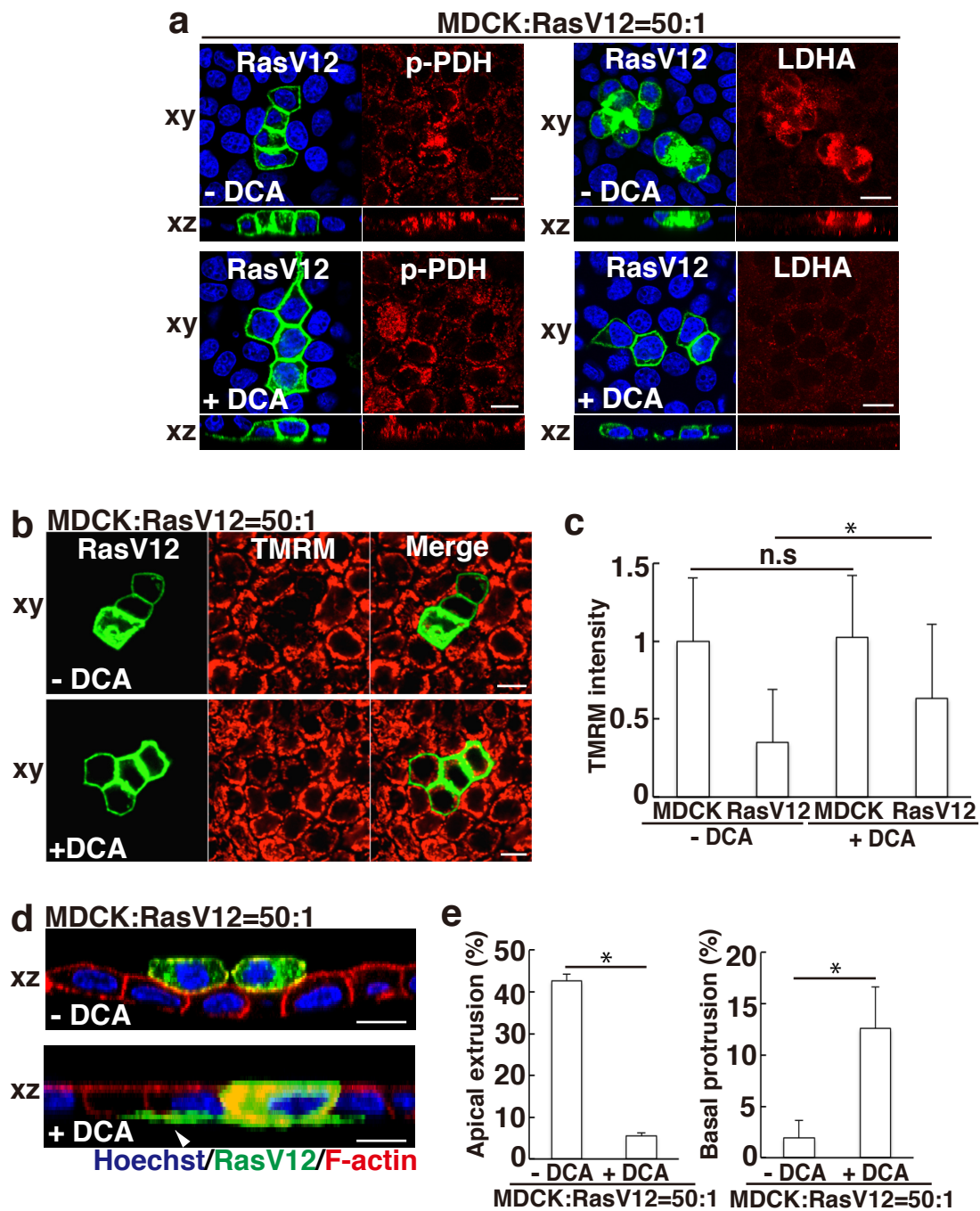


Figure 4 Kon et al.

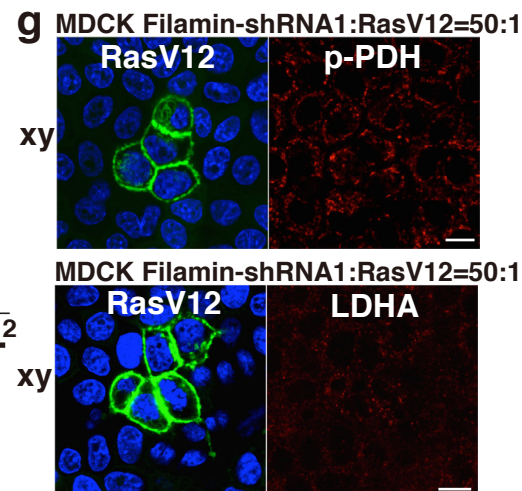
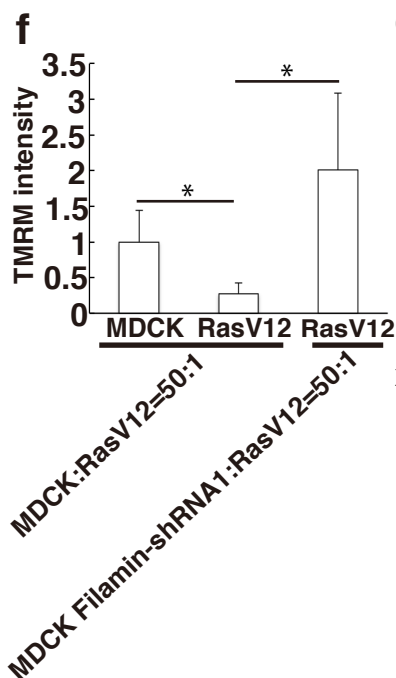
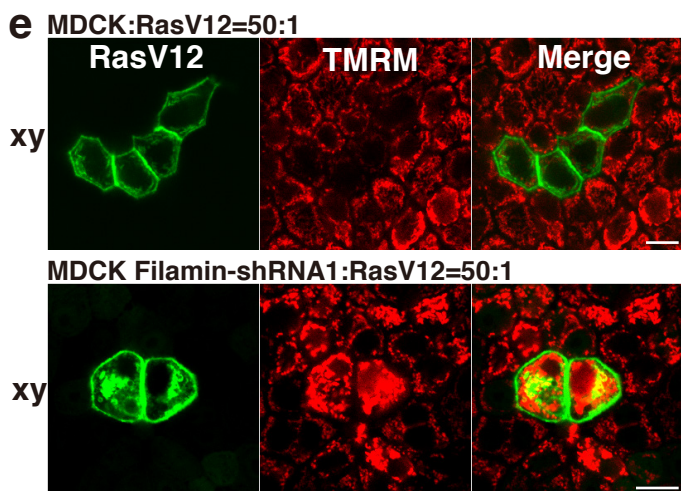
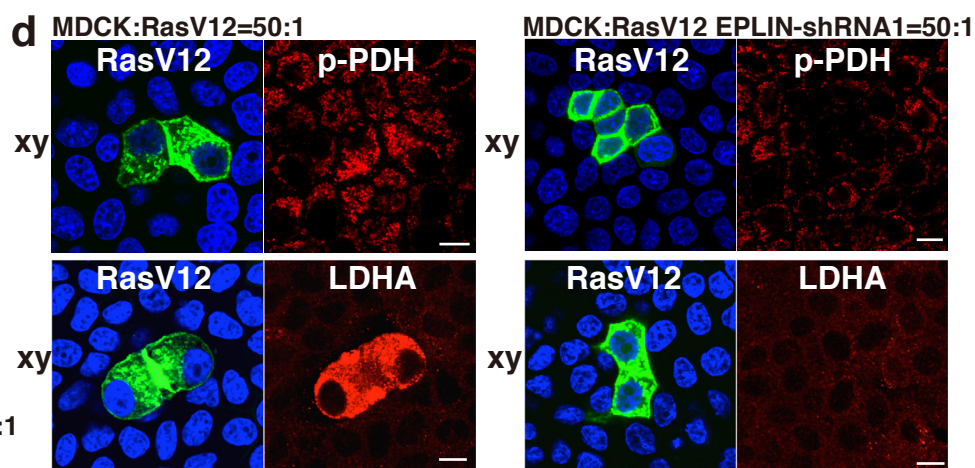
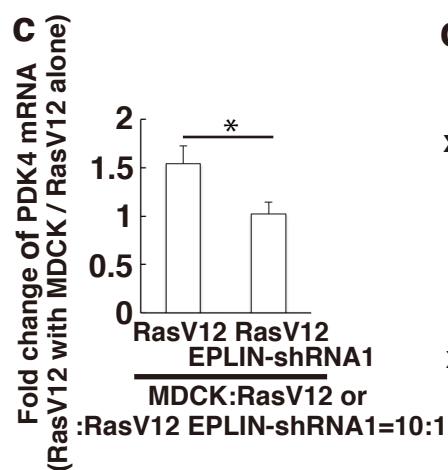
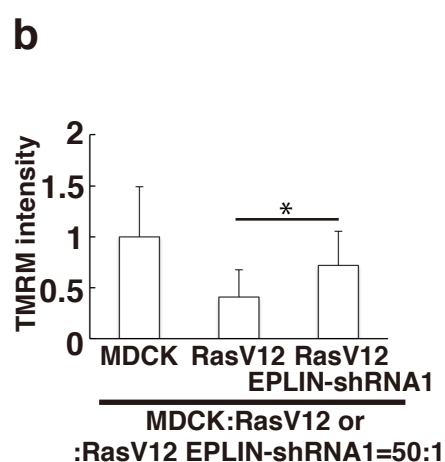
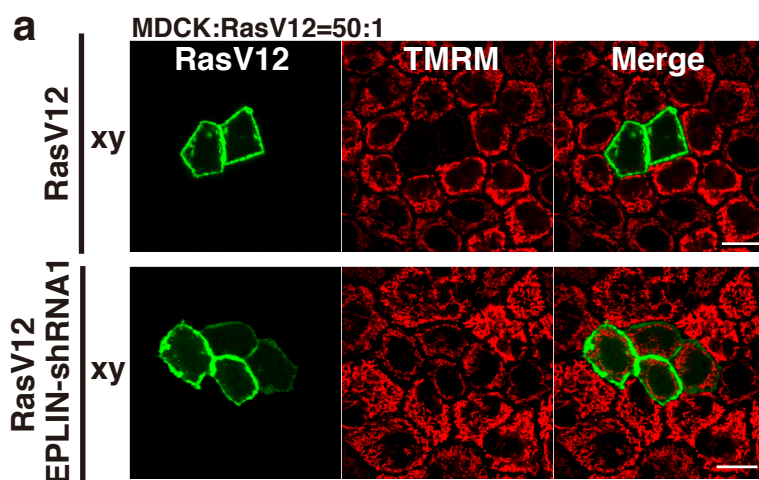


Figure 5 Kon et al.

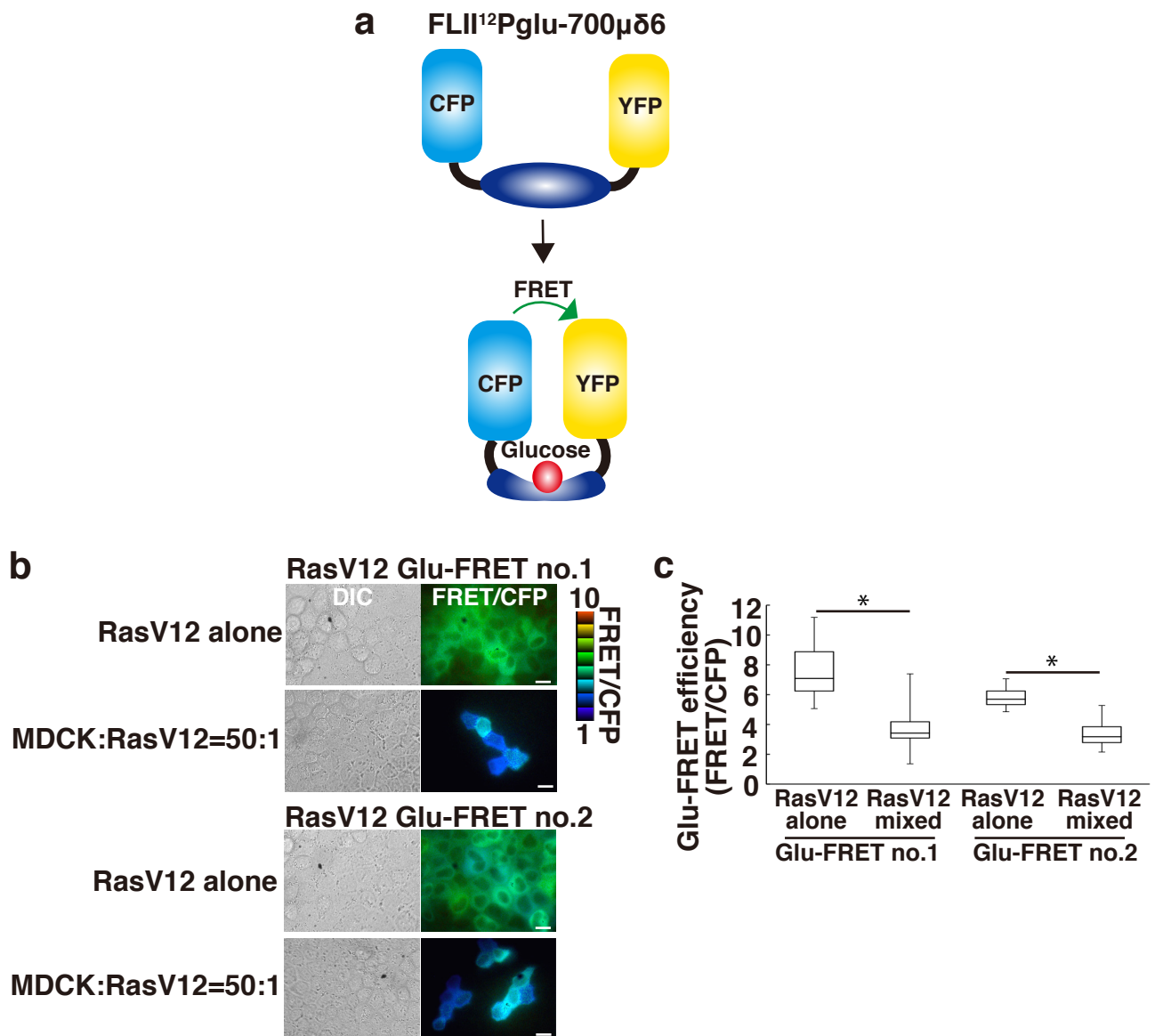


Figure 6 Kon et al.

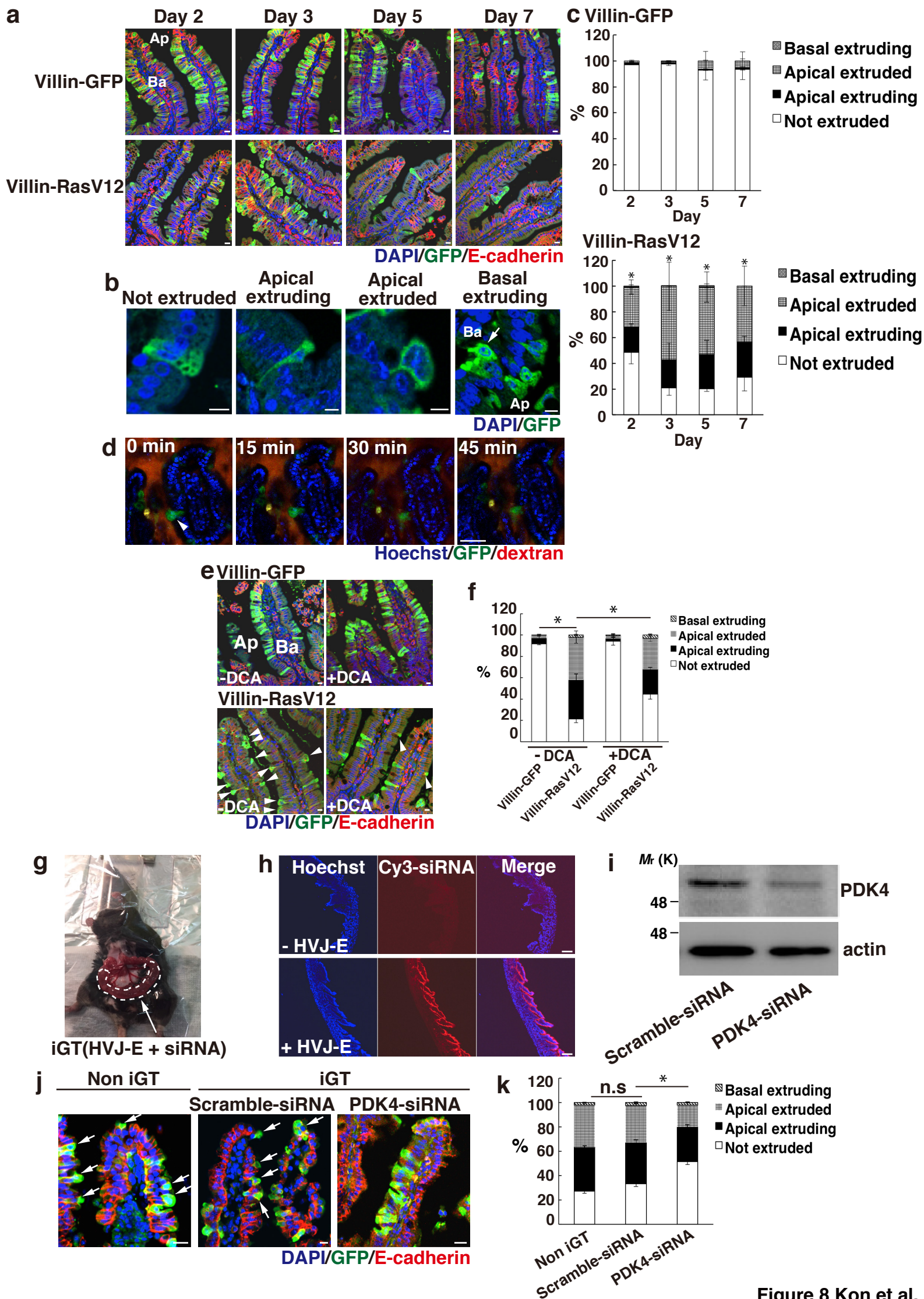


Figure 8 Kon et al.